



# **The influence of the environment on corrosion**

A laboratory-scale analysis

Elisabeth Giaprakis

Thesis submitted for the title of

Master in Nautical Sciences

Promotor: Prof. Dr Geert Potters

Academic year: 2021 - 2022



## Foreword

The most difficult part in writing this thesis was actually to choose the subject that I was going to write about. Several options were presented to me, each as interesting as the other. One of these options was to write about corrosion. After much thought, I decided to join the SOCORRO team, as the subject of corrosion had really caught my attention during my curriculum at the Antwerp Maritime Academy. This choice proved to be the right one as it was beneficial on several levels. By carrying out the experiment discussed in this thesis, I not only learned how to handle certain chemicals and to work in a laboratory, but I also got the opportunity to deepen my knowledge of chemistry, data analysis and statistics, materials science and electrochemistry. In addition thereto, the SOCORRO project being an international project in which many institutions are involved, I have had the chance to meet several people with different scientific backgrounds. That has helped me from a purely practical point of view with the writing of my thesis, but more importantly it gave me an idea of what scientific research is about and it helped me gain clarity on what I would like to achieve professionally.

I would therefore like to thank all the people who guided me in this choice and who contributed to the elaboration of my thesis, and more particularly:

Prof. Dr Geert Potters, my promotor; I would like to thank you for your help and advice, but most especially for your availability, which enabled me to undertake this task in the best possible way.

I would also like to thank Burak Karabulut for the practical execution of the experiment, for all the explanations and documentation provided, but mostly for the investment and enthusiasm shown throughout the writing of my thesis.

## Résumé

Le problème que représente la corrosion est majeur et est donc étudié depuis des années par de nombreux scientifiques. Bien que différentes méthodes aient été développées pour tenter de le contrôler, voire de l'arrêter, les pertes matérielles et économiques liées à ce phénomène demeurent excessivement importantes. Afin de contribuer à la recherche pour la réduction de la corrosion dans l'industrie maritime, une équipe de chercheurs a lancé un projet international appelé SOCORRO, le but étant de développer un système permettant de prévoir le taux de corrosion à attendre sur un certain type de produit. Pour ce faire, des expériences ont été menées sur différents types de métal. Ce mémoire se focalise sur des pièces d'acier de Grade A placées dans un système de purification de l'eau basé sur le principe de Moving Bed Bioreactor. Les paramètres environnementaux dans ce système sont changés fréquemment et des mesures sont prises de manière régulière afin d'en comprendre l'effet sur la vitesse de corrosion. De cette expérience il découle que la vitesse de corrosion de l'acier de Grade A est majoritairement affecté par la température, la conductivité et la salinité de l'environnement. Il existe bien sûr une corrélation avec d'autres paramètres, mais celle-ci est moins forte. Les résultats obtenus par l'analyse statistique faite dans ce mémoire peuvent être utilisés pour la compréhension de l'influence de différents facteurs sur l'acier et contribuent donc directement à la recherche pour la lutte contre la corrosion.

## Abstract

Corrosion is a major problem and has therefore been studied for years by many scientists. Although various methods have been developed to try to control or even stop it, the material and economic losses associated with this phenomenon remain excessively high. In order to contribute to the research for the reduction of corrosion in the maritime industry, a team of researchers has launched an international project named SOCORRO. The aim is to develop a system to predict the rate of corrosion to be expected on a certain type of product. To do this, experiments were conducted on different types of steel. This thesis focuses on Grade A steel coupons placed in a water purification test-system based on the Moving Bed Bioreactor principle. The environmental parameters in the system are changed frequently and measurements are taken regularly to understand the effect on the corrosion rate. As a result of this experiment it was found that the corrosion rate of Grade A steel is mostly affected by the temperature, conductivity and salinity of the environment. There is of course a correlation with other parameters, but it is less strong. The results obtained from the statistical analysis in this thesis can be used to understand the influence of different factors on steel and thus contribute directly to corrosion control research.

# Table of contents

<i>List of figures</i> .....	<i>vi</i>
<i>List of tables</i> .....	<i>viii</i>
<i>List of abbreviations</i> .....	<i>ix</i>
<i>Introduction</i> .....	<i>1</i>
<b>1 Corrosion</b> .....	<b>3</b>
1.1 General definition of corrosion .....	3
1.2 Corrosion mechanisms .....	3
1.3 Factors influencing corrosion .....	4
1.4 Types of corrosion .....	6
1.4.1 General and localized corrosion .....	6
1.4.2 Corrosion in different environments .....	6
1.5 Corrosion and the maritime industry .....	8
<b>2 Test system</b> .....	<b>11</b>
2.1 General description of the water purification system .....	11
2.2 Denitrification process .....	13
2.2.1 Denitrification process in the Moving Bed Bioreactors .....	14
<b>3 Tested specimens</b> .....	<b>16</b>
3.1 Carbon and stainless steels .....	16
3.1.1 Difference in corrosion rate between carbon and stainless steels .....	19
3.2 Description of the tested specimens .....	21
3.3 Forms of corrosion to be expected on each specimen .....	23
<b>4 Measuring equipment</b> .....	<b>24</b>
4.1 The Aquaread 800 environmental probe .....	24
4.1.1 General description of the probe .....	24
4.1.2 Parameters measured by the probe .....	25
4.2 LPR probe .....	26
4.2.1 General description of the probe .....	26
4.2.2 Parameters measured by the probe .....	26
4.2.3 Positioning of the probe in the water purification system .....	27
<b>5 Experimental process</b> .....	<b>29</b>
5.1 Placing of the metal coupons in the bioreactor .....	29
5.2 Preparation of the necessary tools for the statistical analysis .....	30
<b>6 Results and discussions</b> .....	<b>34</b>
6.1 Description of the environmental sensory output .....	34
6.1.1 Temperature .....	34
6.1.2 Conductivity .....	36
6.1.3 Salinity .....	38
6.1.4 Dissolved oxygen .....	40
6.1.5 pH .....	42
6.1.6 Turbidity .....	43

6.1.7	Oxidation reduction potential.....	44
6.1.8	Corrosion rate.....	46
<b>6.2</b>	<b>Correlation analysis .....</b>	<b>54</b>
6.2.1	One-on-one correlation between parameters.....	54
6.2.2	Correlation of each parameter with corrosion .....	57
<b>6.3</b>	<b>Functional analysis.....</b>	<b>61</b>
6.3.1	Pourbaix diagram .....	61
6.3.2	Evans diagram .....	64
<b><i>Conclusion.....</i></b>		<b>68</b>
<b><i>Bibliography.....</i></b>		<b>70</b>

## List of figures

Figure 1	Difference in oxygen content in function of temperature in seawater and fresh water ....	8
Figure 2	Water Purification System Setup.....	11
Figure 3	Working principle of the water purification system .....	12
Figure 4	Stainless steel families .....	17
Figure 5	Self reparation of stainless steel.....	19
Figure 6	Degrading of coating layers over time.....	20
Figure 7	Corrosion rate as a function of chromium percentage .....	20
Figure 8	Multiparameter AP-800 set.....	24
Figure 9	Probe orientation relative to flow.....	27
Figure 10	Positioning of the LPR probe on the holding rack.....	28
Figure 11	Holding rack for metal coupons.....	29
Figure 12	R Script Part 1 - importing packages and data.....	31
Figure 13	R Script Part 2 - General analysis .....	31
Figure 14	R Script Part 3 - Boxplots and correlations.....	32
Figure 15	R Script Part 4 - Principal Components Analysis .....	33
Figure 16	Temperature (°C) measured between 01/04/2021 and 29/06/2021 .....	34
Figure 17	Daily temperature variation (°C) for period 01/04/2021 to 29/06/2021 .....	35
Figure 18	Measured values of temperature (°C) – boxplot .....	35
Figure 19	Conductivity (µS/cm) measured between 01/04/2021 and 29/06/2021 .....	36
Figure 20	Daily variation of conductivity (µS/cm) for period 01/04/2021 to 29/06/2021.....	37
Figure 21	Measured values of conductivity (µS/cm) – boxplot .....	37
Figure 22	Salinity (PSU) measured between 01/04/2021 and 29/06/2021 .....	38
Figure 23	Daily variation of salinity (PSU) for period 01/04/2021 to 29/06/2021 .....	39
Figure 24	Measured values of salinity (PSU) – boxplot .....	39
Figure 25	Dissolved oxygen (mg/L) measured between 01/04/2021 and 29/06/2021.....	40
Figure 26	Daily variation in dissolved oxygen content (mg/L) for period 01/04/2021 to 29/06/2021.....	41
Figure 27	Measured values of dissolved oxygen concentration (mg/L) – boxplot .....	41
Figure 28	pH values measured between 01/04/2021 and 29/06/2021.....	42
Figure 29	Measured values of pH – boxplot .....	42
Figure 30	Turbidity (NTU) measured between 01/04/2021 and 29/06/2021.....	43
Figure 31	Measured values of turbidity (NTU) – boxplot .....	44
Figure 32	Oxidation reduction potential (mV) measured between 01/04/2021 and 29/06/2021 ....	45
Figure 33	Measured values of ORP (mV) – boxplot.....	45
Figure 34	Corrosion rate (mm/y) measured between 01/04/2021 and 13/07/2021.....	46

Figure 35 Corrosion rate (mm/y) with filters - measurements from 01/04/2021 to 13/07/2021 a: measured data with 1 <sup>st</sup> derivative filter; b: measured data with Savitzky-Golay filter; c: measured data with EMA filter; d: measured data with all filters combined .....	48
Figure 36 Statistical analysis of the filtered data.....	49
Figure 37 Potentiodynamic measurement .....	50
Figure 38 Mass loss measurements - coupons before and after cleaning.....	51
Figure 39 Mass loss of coupons after each cleaning cycle.....	53
Figure 40 Comparison of LPR probe method, potentiodynamic test and mass loss measurement.	54
Figure 41 Correlation between the parameters measured by the environmental probe .....	55
Figure 42 Screenplot - total number of principal components obtained from PCA.....	58
Figure 43 Corrosion rates biplot - PC1 & PC2.....	59
Figure 44 Corrosion rates biplot - PC1 & PC3.....	60
Figure 45 Corrosion rates biplot - PC2 & PC3.....	61
Figure 46 Corrosion rate plotted on a Pourbaix diagram .....	64
Figure 47 Linear polarization curve .....	65
Figure 48 Tafel plot for predicting corrosion rate .....	66
Figure 49 General aspect of an Evans diagram .....	67

## List of tables

Table 1	Differences between Tile-drained agricultural effluent and greenhouse effluent.....	14
Table 2	Charpy test indicator .....	19
Table 3	Chemical composition of S235JR carbon steel Values are given in molar fraction.....	21
Table 4	Chemical composition of S355J2 carbon steel .....	21
Table 5	Composition of 316L stainless steel in percentage by mass .....	22
Table 6	Mechanical properties of 316L stainless steel .....	22
Table 7	Parameters measured by the environmental probe.....	25
Table 8	Weight of coupons before first immersion .....	30
Table 9	Weight of coupons after each cleaning cycle.....	51

## List of abbreviations

<i>EMA</i>	<b>Exponential Moving Average</b> Type of filter used in statistical analysis, based on the moving average technique (technique whereby data is analysed by creating a series of averages of different subgroups of the initial database).
<i>GDP</i>	<b>Gross Domestic Product</b> Measure of the value added created through the production of goods and services in a country.
<i>KULeuven</i>	<b>Katholieke Universiteit Leuven</b> State funded catholic research university in Leuven, Belgium. This university ranks among the top 100 universities in the world.
<i>LPR</i>	<b>Linear Polarisation Resistance</b> Indicates the resistance of a system to linear polarisation. LPR tests can be used to determine corrosion rate.
<i>MBBR</i>	<b>Moving Bed Biofilm Reactor</b> Type of wastewater treatment process consisting of an aeration tank with plastic carriers providing a surface where biofilm can grow.
<i>MIC</i>	<b>Microbial Induced Corrosion</b> Also called Microbiologically Induced corrosion, it is a type of corrosion caused by the presence of microorganisms on the surface of corroding materials.
<i>NTU</i>	<b>Nephelometric Turbidity Unit</b> Unit used for the measurement of turbidity, as prescribed by the Environmental Protection Agency.
<i>ORP</i>	<b>Oxidation Reduction Potential</b> Measure of ability of a liquid or biochemical system to oxidize (lose electrons) or reduce (gain electrons).
<i>PCA</i>	<b>Principal Components Analysis</b> Statistical analysis method used to determine the levels of correlation between different parameters.
<i>pH</i>	<b>Potential of Hydrogen</b> Scale used to specify the acidity or basicity of an aqueous solution.
<i>PSU</i>	<b>Practical Salinity Unit</b> Unit used to measure salinity of a solution.

## Introduction

Corrosion is a major problem affecting metal structures, causing enormous losses and thus taking a huge toll on the global economy. Indeed, the direct cost caused by corrosion is estimated at \$276 billion per year in the United States (Koch, Brongers, Thompson, Virmani, & Payer, 2002). In China, corrosion-related costs are estimated at \$310 billion (Hou et al., 2017), i.e. 3.34% of the Gross Domestic Product (GDP). Globally, the amount reaches 2.5 trillion, which corresponds to 3.4% of the GDP. All this without counting the indirect costs linked to corrosion, which also represent a significant share of the world's GDP. By using current means of corrosion control, it would be possible to reduce the overall cost by 15 to 35%, but the remaining cost would still be very high (Koch et al., 2016).

Of course, beyond the financial aspect, corrosion has effects on many other levels as well. For example, the loss of steel and thus the demand for the production of new steel to replace defective parts has an impact on global warming. Beyond that, corrosion also represents a health and safety hazard for people coming into direct contact with rusty parts.

This situation affects many industries, one of them being the maritime industry, where steel is used not only for the construction of ships, but also for all kinds of port, offshore and underwater structures and installations.

Although there is a lot of research going on and several approaches already exist, additional help and a fresh look at the situation are always welcome. For this reason, an INTERREG 2 Seas project involving 15 partners has been established. This project, called “SOCORRO – Seeking out corrosion (before it is too late)” (Interreg 2S07-031, [www.socorro.eu](http://www.socorro.eu)), is led by academic and industrial partners from Belgium, France, the Netherlands and Great Britain, and aims to create a new methodology for the determination and control of the corrosion of immersed metal parts.

The ultimate goal of this project is to create an artificial intelligence system capable of determining the rate of corrosion to be expected on different types of steel, in order to know whether it makes sense to use the part or if it will only lead to losses. To do so, tests are carried out on several types of steel immersed in different solutions for which the environmental parameters are changed regularly. The observations and data gathered throughout these experiments are then studied and analysed by various researchers. This,

together with the knowledge about corrosion that is already available at the moment, will make it possible to calculate the risk of corrosion as a function of the environment to which the structures are exposed.

As part of Work Package 1 (Data Analysis) of the SOCORRO project, an experiment was conducted on Grade A steel coupons placed in a water purification test-system at the Katholieke Universiteit Leuven. It is that experiment that will be analysed and described throughout this thesis. In order to better understand the corrosion mechanism and to be able to understand the influence of the environment on it, a brief description of the physicochemical process will be given in Chapter 1, followed by a non-exhaustive list of important environmental factors to be taken into consideration when studying corrosion. In Chapter 2, the role that corrosion plays in the maritime industry will be discussed. After setting the context for this thesis, a description of the water purification system and the type of metal used will be given in Chapters 3 and 4, as well as a description of the different probes used to collect data as part of Chapter 5. This will directly be followed by a description of the experiment. The results will then be discussed and analysed in an attempt to obtain relevant conclusions that may be useful for the project (Chapter 6).

# 1 Corrosion

## 1.1 General definition of corrosion

Corrosion, from the Latin *corrodere*, is the chemical and physical degradation of a material exposed to severe environmental conditions. In the case of metals, it occurs as a result of their tendency to return to their most stable thermodynamic state (Pedefferri, 2018).

Metals are often produced, with the addition of a certain amount of energy, from ores. Their metallic form is therefore only temporary. When these metals are exposed to their environment, they tend to revert to their original state, i.e. to their ore state (Roberge, 2008).

The *International Union of Pure and Applied Chemistry* (Heusler, Landolt, & Trasatti, 1989) defines corrosion as follows :

*Corrosion is an irreversible interfacial reaction of a material (metal, ceramic, polymer) with its environment which results in consumption of the material or in dissolution into the material of a component of the environment. Often, but not necessarily, corrosion results in effects which are detrimental to the usage of the material considered. Exclusively physical or mechanical processes such as melting or evaporation, abrasion or mechanical fracture are not included in the term corrosion.*

## 1.2 Corrosion mechanisms

There are two different mechanisms for metal corrosion (Heusler et al., 1989).

The first, called high-temperature corrosion, is a mechanism that applies particularly to metals exposed to hot gases. This phenomenon usually takes place in turbines or boilers and does not require the presence of an electrolyte liquid, which is why it is sometimes called dry corrosion (Caballero, 2022).

The second mechanism is aqueous corrosion which, as the name implies, applies to metals exposed to an electrolyte fluid. It is the main corrosion process at room temperature or at lower temperatures.

Although these two processes are distinct, there are some environments in which a corrosive attack combines both types (Pedefferri, 2018).

### 1.3 Factors influencing corrosion

As corrosion is a reaction of metals to their environment, it seems obvious that it is influenced by both intrinsic metal factors as well as environmental factors.

At the metal level, the most important factor is the composition of the alloy, which is characterised, among other things, by the presence of impurities, the crystalline structure of the metal and the various constituents used.

In order to increase the corrosion resistance of a metal, the composition of the metal must be changed (Pedefferri, 2018). This can be done by different processes. One is to add a more noble element, such as chromium or copper, to increase the nobility of the alloy itself. Another process would be to add impurities, i.e. elements containing a high hydrogen overpotential.

From an environmental perspective, several factors have been noted to affect the rate of corrosion.

Conductivity, for example, is a property of materials and of the liquid or gaseous environment surrounding those materials that characterises their ability to conduct heat as well as electricity. Due to the presence of ions, the fluids surrounding the metal, known as electrolytes, have a certain electrical conductivity. This conductivity has a direct influence on corrosion: the higher it is, the higher the corrosion rate will be, provided a cathodic process is present.

Another important factor is the pH of the environment in question. Some metals are more susceptible to corrosion in acidic solutions, while others are more likely to corrode in alkaline or neutral solutions. Noble metals are resistant to corrosion in both basic and acidic solutions.

A third factor is temperature, which is directly related to the rate of a chemical reaction (electrochemical reactions generally occur faster at higher temperatures). Therefore, corrosion being a reaction between three reactants (namely metal, dioxygen and water), an increase in temperature implies an increase in the rate of corrosion.

Similarly, an increase in pressure implies an increase in the rate of corrosion. This increase in pressure can be found in environments to which certain gases such as CO<sub>2</sub> or H<sub>2</sub>S are added.

In addition to all these elements, there is also the presence of bacteria, for example sulphate-reducing bacteria which are involved in microbial induced corrosion (MIC).

These factors are obviously not an exhaustive list. The principle of corrosion is complex and many other elements influence the environment in which it takes place, such as the presence of oxidants, galvanic coupling, condensation, flow regime, and many others (Roberge, 2008).

It is important to note that some of these factors may be interdependent, i.e. a change in one of them will directly influence one of the others. In order to get a clearer idea of the complexity of this interdependence, some examples will be discussed.

The first important parameter to deal with is temperature, which has an influence at different levels. In addition to its influence on corrosion rate, an increase in temperature implies an increase in conductivity and thus a reduction in resistivity which is, by definition, the reciprocal of conductivity (Chang, Sommerfeldt, Carefoot, & Schaalje, 2011). However, in a completely contradictory manner, an increase in temperature causes a decrease in the concentration of dissolved oxygen and therefore a decrease in the rate of corrosion. Thus, temperature influences the corrosion rate upwards through its impact on the reaction rate and on conductivity, but it also influences corrosion downwards through its impact on the dissolved oxygen level.

Two other parameters to consider are salinity, which is a measure of the total concentration of dissolved salts in water, and the concentration of chloride ions, the anions most commonly found in seawater and brackish water. The relationship between these two parameters can be represented using Equation 1 for determining the salinity of seawater and brackish water based on their chloride concentration (Vernier Software and Technology, n.d.).

$$\text{salinity (ppt)} = 0.0018066 \times Cl^- \text{ (mg/L)} \quad (\text{Eq. 1})$$

In addition thereto, there is a relationship between salinity and dissolved oxygen content (as will be discussed in paragraph 1.4.2). Indeed, when the salinity of water increases, its capacity to dissolve oxygen decreases (Fondriest Environmental, Inc., 2013).

These examples emphasise the importance of studying the correlation between each of those parameters in order to understand their total influence on the corrosion rate.

## 1.4 Types of corrosion

The corrosion process can be divided into several types. The method of classification can be based on the size of the corroded surface or on the environment to which the element is exposed.

### 1.4.1 General and localized corrosion

When considering the size of the corroded surface, two categories can be distinguished (Groysman, 2010).

The first category is general corrosion, also called uniform corrosion. Here, the corrosion attack is evenly distributed over the entire metal surface and can be measured by the mass loss per unit area.

The second category is localised corrosion, which applies only to a part of the metal surface. It can be found in different forms, such as grooving corrosion, pitting corrosion, crevice corrosion, galvanic corrosion, MIC, erosion corrosion, stress corrosion, stray current corrosion, intergranular corrosion, dealloying hydrogen-induced cracking, hydrogen blistering. Some of these forms will be further discussed in point 3.3.

### 1.4.2 Corrosion in different environments

With regard to classification on the basis of the environment, three main categories can be distinguished: corrosion in water, atmospheric corrosion and soil corrosion (Groysman, 2010; Pedferri, 2018; Roberge, 2008). As this thesis deals with the corrosion of metals used in industrial processes related to the maritime industry, it seems obvious that only the category of corrosion in water should be further detailed.

As soon as a cathodic process can take place, i.e. when hydrogen ions are reduced to form hydrogen gas, water is considered corrosive to metals. The cathodic reactant is therefore one of the factors influencing the corrosion of metals in water. This reactant is mainly dissolved oxygen, which influences the corrosion rate. Its solubility depends on salinity, fluid dynamic regime and temperature.

Another important factor is the presence of  $\text{Ca}^{2+}$  and  $\text{Mg}^{2+}$  ions, which contribute to the formation of calcareous deposits. This content is called water hardness and is presented in three forms: total hardness being the total content of these ions in a certain quantity of water, permanent hardness being the quantity remaining after boiling and filtration of the water, and temporary hardness being the difference between the two previous forms. The harder

the water, the richer it is in  $\text{Ca}^{2+}$  and  $\text{Mg}^{2+}$  ions. These ions form a calcareous deposit on the surface of the immersed metal and therefore act as a protective barrier by reducing the permeability of the metal and thus the possibility of diffusion of oxygen and other ions favourable to corrosion. As this diffusion is reduced, so are the rates of long-term corrosion (De Baere et al., 2021; Duran, 2013). This tendency of the water to create a calcium carbonate layer on the surface of the metal is called the scaling tendency, and the calcareous deposit can be referred to as scale (Reid, 2020).

Other factors to be taken into account are pH, temperature, resistivity and the presence of bacteria (Alahmad, 2004).

A different value for each of these parameters can lead to different chemical compositions and physical properties, which is why several types of water can be distinguished, ranging from fresh water, through potable water, distilled water and industrial water, to sea water. It is obvious that corrosion will not be the same depending on the type of water considered (Groisman, 2010). In seawater and brackish water, salinity exceeds 2 g/L by definition, but generally varies around 35 g/L. This salinity, together with temperature and barometric pressure, influences the concentration of dissolved oxygen, which as mentioned earlier is the most common reactant causing corrosion in water (Pawlowicz, 2013).

An increase in barometric pressure leads to an increase in dissolved oxygen content. An increase in both temperature and salinity, on the other hand, leads to a decrease in dissolved oxygen content. Warm seawater therefore contains less dissolved oxygen than cold fresh water (as shown in Figure 1). However, the first type is still more corrosive. This is because seawater contains more ionic species than fresh water. This concentration directly influences the conductivity, and that of seawater is 100 to 200 times higher than that of fresh water (Pedefferri, 2018). As mentioned in point 1.3, the higher the conductivity, the higher the corrosion rate.

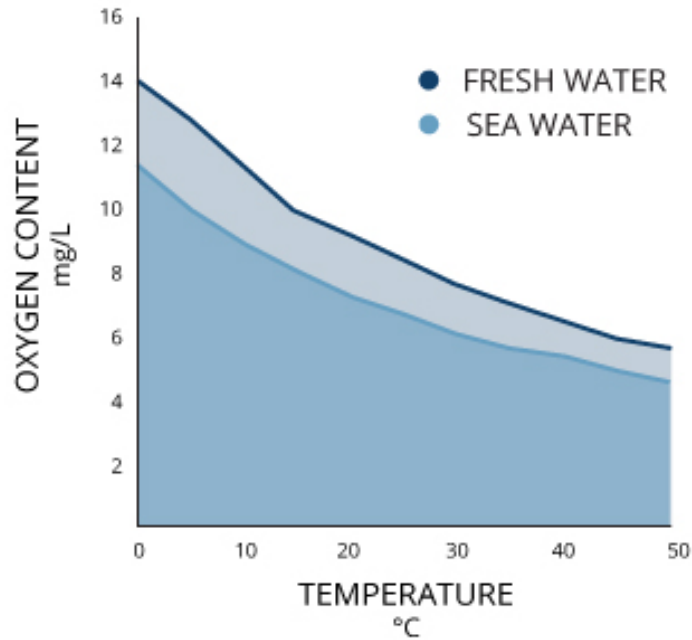


*Figure 1 Difference in oxygen content in function of temperature in seawater and fresh water*

(Fondriest Environmental, Inc., 2013)

### 1.5 Corrosion and the maritime industry

Several aspects of the maritime sector are affected by corrosion. The most obvious, and the one that many people would tend to think of, is the maritime fleet (ships). Although these steel giants are indeed prone to rusting, they are far from being the only victims. Port facilities, offshore structures and underwater pipes, among others, are also to be considered (DNV, 2021).

The problem of corrosion is therefore a large-scale one and it has several undesirable consequences, the first being a huge budgetary cost. Indeed, each of the structures used in the maritime industry has a certain life expectancy, that of merchant ships being generally around 25 years (Dinu & Ilie, 2015). The corrosion process starts as soon as the metal part in question comes into contact with sea water, and it develops and worsens enormously over the years. In this way, huge sums have to be paid for the repair and replacement of these structures which are weakened and sometimes do not last until their expected design life. This design life represents the period of intended use for the structure, including minor repairs, and can be calculated using the lifetime safety factor method, which is based on probabilistic degradation models that take into account the decrease in structural resistance caused by various environmental loads (Landolfo, Cascini, & Portioli, 2010; Sarja, 2000).

To look at a concrete example, wind farms are one of those aspects of the maritime sector affected by corrosion. Offshore wind turbines have a life expectancy of 20 years and the repairing cost of such structures is so high that it is most often unrealistic to even consider it. Of course, before talking about repairs, it would seem logical to consider limiting the damage by having a system of regular inspections. However, these wind turbines are strategically placed in high wind areas and rough weather conditions. These inspections are therefore very dangerous and require the work of qualified and certified personnel, which also comes with a price (Mathiesen, Black, & Gronvold, 2016). This example emphasises the fact that it is not easy to limit corrosion and that the costs mentioned are not only limited to material replacement costs, but that several other problems are linked to it.

To get an idea of the order of magnitude of the costs involved in corrosion damage, it is worth looking at a US study on the annual cost of corrosion for Army vehicles and Navy ships (Herzberg et al., 2006). At the time of the study, more than \$1.35 billion was spent annually for Navy ships on depot costs alone, i.e. costs related to the maintenance of equipment on a large scale (rebuilding certain parts, modifications, testing). In addition, there are man-hours for smaller-scale inspections and repairs, the use of equipment, training of qualified personnel, and much more.

Beyond these costs specifically related to military ships, a 2002 study found that \$2.7 billion was spent each year as a result of corrosion in the shipping industry. That amount was divided between new ship construction, structural maintenance and repair and corrosion-related downtime (Koch et al., 2002).

To this date, the only solutions used to try to reduce corrosion are regular inspections and the application of coatings to structures in contact with water. However, none of these measures are effective as the costs associated with corrosion are still extremely high. Yet one sixth of these costs could be avoided if the problem was tackled more effectively (Koch et al., 2016).

In order to better understand the problem and be able to approach it in a more effective way so as to potentially be able to, if not eliminate it, at least avoid it as much as possible, it is interesting to look at the causes of corrosion and at the reason why the corrosion rate increases over time. Indeed, predicting the corrosion rate that can be expected on a product

allows to see if its design life will be met, which also gives an idea of the impact on a company's economy if they decide to build a certain structure.

As explained in paragraph 1.3, there are different microbial and physicochemical parameters that influence corrosion. Several relationships exist between these parameters, but they are not linear, which makes them too complex to be modelled. It is therefore necessary to use artificial intelligence that could translate the measurements and interactions of environmental factors into a corrosion risk.

To do this, the influence of these parameters on different types of steel should be studied and data should be collected for each of the parameters. The information obtained should then be analysed in order to be correctly understood, after which the necessary modifications could be made to the measuring system used. As a result, an algorithm can be developed. This algorithm will be able to predict the corrosion rates and speeds to be expected on different types of metal, and therefore on different structures.

In order to contribute to the development of this algorithm, experiments were conducted on metal coupons placed in a water purification system as described in paragraph 2.1.

## 2 Test system

### 2.1 General description of the water purification system

This thesis focuses on simulations carried out on different metal coupons placed in a water purification system located at the Katholieke Universiteit Leuven (KULeuven), Campus De Nayer (Sint-Katelijne-Waver). It is based on a Moving Bed Bioreactor (MBBR) process which aims to remove nitrogen from the drainage water of a greenhouse belonging to an agricultural company located in Putte (Boeckeaert, 2019).

The lab-based water purification test system (Figure 2) consists of four double-walled recipients (bioreactors). Two of the four reactors are kept at a temperature of 5-8°C (figure 2 a, b) while the two others are at room temperature (figure 2, c, d). Each reactor contains biofilm carriers within which denitrifying bacteria grow. These bacteria will serve to reduce the nitrate to nitrogen gas.



*Figure 2 Water Purification System Setup.  
a, b: reactors kept at 5-8°C; c, d: reactors kept at room temperature*

Apart from the temperature, all parameters are identical for both subsystems. The pH, for example, is maintained at an almost neutral level (varying from 6 to 9). For ease of reference and to match the diagram in Figure 3, the system on the left will be referred to as MBBR 1 and the system on the right as MBBR 2.

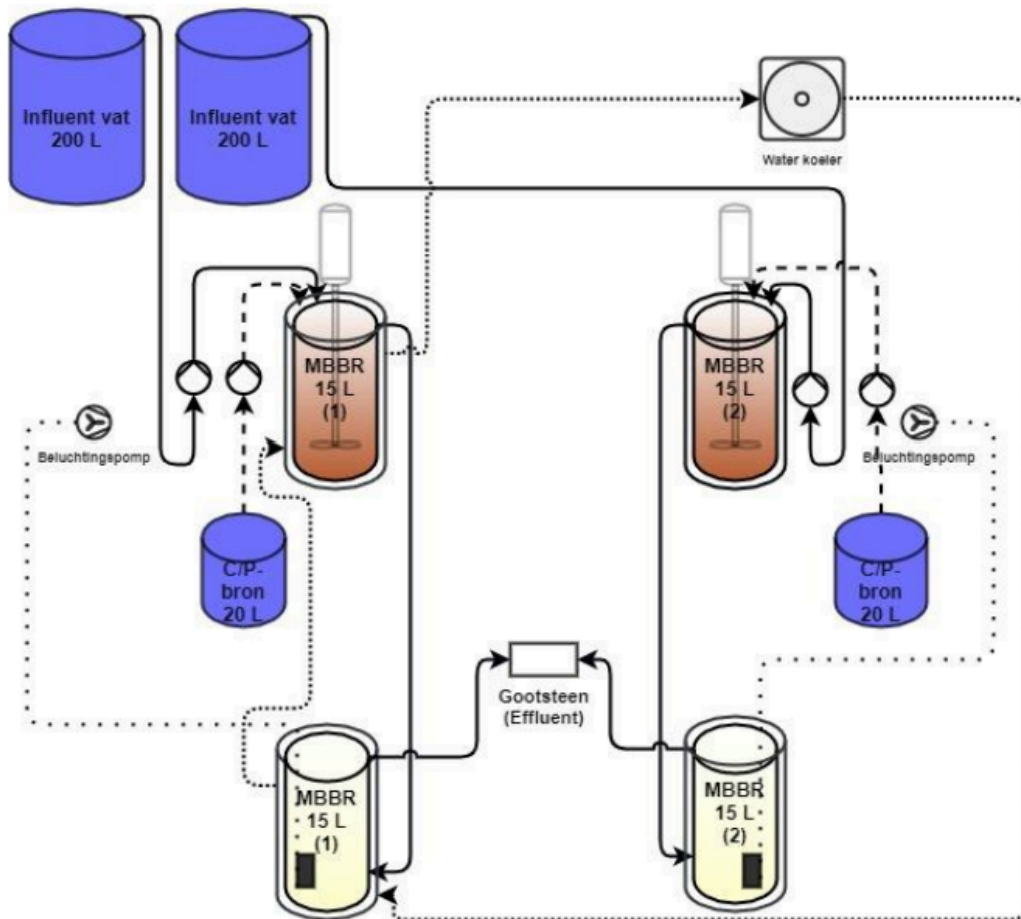


*Figure 3 Working principle of the water purification system*

(Van Praet, 2020)

Depending on the type of purification desired and on how the biofilms are moved through the bioreactors, the MBBR can be operated by an aerobic, anoxic or anaerobic process. Since this system aims to denitrify potassium nitrate, an anoxic MBBR was placed in series with an aerobic MBBR for both subsystems. The difference in oxygen content is one of the reasons why the biofilm carriers vary in colour, as is clearly visible in Figure 2.

In the anoxic MBBRs, which are the ones on the top-level of the setup, the biofilm carriers are brought into motion in a circular flow pattern using a hyperboloid mixer, which is a type that avoids the sedimentation of particles and turbulence at the water surface. The wastewater is pumped from a drainage well via a pulse pump, also called influent pump, and

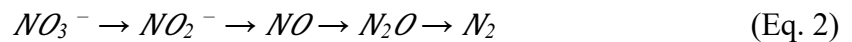
is fed to the anoxic reactors. In addition, carbon is added as an energy source to maintain denitrification reaction. Phosphorus is also added in very small quantities to ensure biomass growth. This phosphorus is absorbed by the biocarriers so there is no phosphorus outflow in the effluent. By means of an overflow, the wastewater is brought from the anoxic reactors to the aerobic MBBRs, in which the biofilm carriers are set in motion by means of an air pump. Both MBBR 1 and MBBR 2 aerobic reactors are connected to a gutter via an overflow to discharge the effluent from both systems (Boeckaert, 2019; Van Praet, 2020).

In order to ensure sufficient space for water and to allow the biofilm carriers to move freely, the reactors were only filled to 30% with carriers. Also, the biofilm carriers have a lower density than water, which causes them to float. In order to keep them in the reactors, a sieve was placed at each outlet (Ødegaard, 2006; Van Praet, 2020).

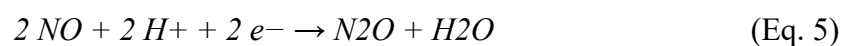
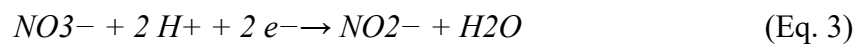
## 2.2 Denitrification process

The drainage water contains a high concentration of nitrate (150-300 mg NO<sub>3</sub>-N/L) as well as a high concentration of phosphate. The denitrification process takes place under anoxic conditions using heterotrophic bacteria developed on the carriers. When the bacteria enter the environment, they satisfy their oxygen requirement by deoxygenating the nitrate ions which are used as electron acceptors. In order for this microbiological activity to take place, the bacteria require energy, which is provided by a carbon source (Van Aken, 2021).

In a denitrification process, nitrogen gas is not produced at once, but various intermediate steps occur before the nitrate is completely denitrified. The sequence from beginning to end product is as follows;



These intermediate products are obtained by several reactions, namely : the reduction of nitrate to nitrite as indicated by Equation 3, the reduction of nitrite to nitric oxide as indicated by Equation 4, the reduction of nitric oxide to nitrous oxide as indicated by Equation 5, and the reduction of nitrous oxide to dinitrogen as indicated by Equation 6.



These reactions can be expressed as a redox reaction representing the whole denitrification process, as indicated by Equation 7.



Only an oxygen-deficient environment makes denitrification possible. The reason for this is that if oxygen is supplied to the reactors, it will consume the carbon which is meant to act as an energy source. In addition to this low oxygen environment, several conditions must be met for denitrification to take place in the best possible way : the pH should be between 6 and 8, a source of easily biodegradable carbon should be present, as well as a source of phosphorus, and the temperature should be between 5 and 30°C.

Based on the description of the system given in paragraph 2.1, it is obvious that all those requirements have been met in the setup used for the denitrification experiment at the KULeuven.

Another important factor to take into account is that the nitrate concentration can impact the process. Indeed, for nitrate concentrations above 3 mg/L, the rate of denitrification will depend entirely on the amount of carbon available (Boundless, 2021; Ødegaard, 2006), which is why nitrate concentration is kept below this value in the bioreactors.

### 2.2.1 Denitrification process in the Moving Bed Bioreactors

The goal is to treat the drainage water from agricultural water and removing nitrate by converting it into nitrogen gas by using biological denitrification in anoxic conditions.

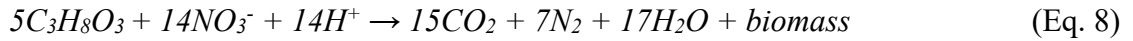
There are two different types of effluent being treated. The first type is drainage water from tile-drained fields, which has a limited nitrate concentration and has a high flow rate but only flows in winter conditions (which is why the temperature of the system is kept around 5°C). The second type is the greenhouse effluent, which has a higher nitrate concentration and a low flow rate. This type flows during the whole year (Boeckaert, 2019; Van Aken, 2021; Van Praet, 2020). The differences between these two types are summarized in Table 1.

**Table 1** *Differences between Tile-drained agricultural effluent and greenhouse effluent*

(Van Aken, 2021)

	<b>Tile-drained agricultural fields</b>	<b>Greenhouse effluent</b>
<b>NO<sub>3</sub> concentration</b>	50 – 200 mg/L	100 – 400 mg/L
<b>Flow rate</b>	High: 7.5 – 15 m <sup>3</sup> /day	Low: 3 m <sup>3</sup> /day
<b>Period of the year</b>	November - April	Whole year

In order to treat both types of effluent, the following reaction (Equation 8) is used;



where  $5C_3H_8O_3$  represents the glycerol-based carbon source that needs to be added to maintain the denitrification process;  $14H^+$  represents the pH increase; biomass represents the biomass produced, which is very limited because it is absorbed by the biofilm carriers. However, this biomass concentration is very active, meaning that there is a lot of surface area that can be used to intensify the denitrification reaction and therefore limit the ecological footprint of the installation.

As mentioned in paragraph 2.2, the denitrification does not take place at once. There are several intermediate steps before passing from  $14NO_3^-$  to  $7N_2$  as follows;



All intermediates can be used for other applications, but at  $7N_2$  there is no recovery possible due to the gaseous nature of the product.

### 3 Tested specimens

As S355, Grade A and 316L steels are the types of steel that are most often used in the maritime industry and for construction works, it seems appropriate to focus on these metal types for the corrosion simulation experiment. The two former types are carbon steels while the latter is a stainless steel. Only one type of steel (Grade A) has been evaluated for the purpose of this thesis. The two other types will be used for a future thesis.

#### 3.1 Carbon and stainless steels

**Stainless steels** are a type of metal alloys mainly composed of iron. Their particularity is that they contain a large amount of chromium, which makes them more resistant to heat and corrosion. This will be further discussed in section 3.1.1.

These alloys can be divided into five families based on their chemical composition, and therefore on their crystal structure (Cunat & Davidson, 1998).

Austenitic stainless steels are the largest family. As the name suggests, they have an austenitic structure, i.e. a face-centred cubic atomic structure, which is obtained by adding nickel (8 to 11%) or manganese and nitrogen to the alloy. This composition means that they have the same microstructure at all temperatures and cannot be strengthened by heat treatment. In addition to this, they usually contain between 17 and 18% chromium which makes them highly resistant to corrosion. They also have a high ductility and are therefore very weldable.

Ferritic steels, on the other hand, have a body-centred cubic structure like carbon steels. They contain between 10.5 and 18% chromium and practically no nickel. These alloys also have the same microstructure at all temperatures and therefore cannot be strengthened by heat treatment. They are relatively ductile, but less than austenitic steels. They also have good corrosion resistance.

A combination of these two crystal structures leads to a third family, that of duplex steels (otherwise known as austenitic-ferritic stainless steels). These alloys contain between 20 and 26% chromium, between 1 and 8% nickel and up to 5% molybdenum. Their yield strength is twice that of austenitic steels, but they are less formable, although they possess fairly good ductility. Due to their mixed microstructure, they are more resistant to stress corrosion cracking.

A fourth family is that of martensitic stainless steels. They have the same crystalline structure as ferritic and carbon steels. They contain a great amount of carbon and can therefore be strengthened by heat treatment. They are less ductile than the three previous families and are less weldable. They have a low chromium content which makes them not very resistant to corrosion.

The last family is precipitation hardening stainless steels. These alloys are divided into three groups: martensitic, semi-austenitic and ferritic. Their corrosion resistance is comparable to that of austenitic steels, and therefore superior to that of martensitic steels.

A summary of the characteristics of the first four families can be found in Figure 4.



*Figure 4 Stainless steel families*

([www.worldstainless.org](http://www.worldstainless.org))

**Carbon steel**, on the other hand, is an iron alloy containing an amount of carbon ranging from 0.05% to 2.1%. Although this addition of carbon increases the hardness of the steel, it also has an effect on the yield strength. Adding too much makes the steel less ductile and subject to permanent deformation. It is therefore important not to exceed the 2.1% limit, above which the steel is no longer weldable and therefore no longer usable for construction (Eberhart, 2003; González-Viñas & Mancini, 2004).

Based on carbon content, different types of carbon steel can be distinguished (Ashby, Shercliff, & Cebon, 2007; González-Viñas & Mancini, 2004; Lamarsh & Baratta, 2001).

Low carbon steel has a carbon content of less than 0.1% and is soft and malleable, meaning it can easily be deformed.

Mild steel has a carbon content of 0.1 to 0.25% and is the most common form of steel. It is malleable and ductile making it easy to weld, but has a low tensile strength, meaning that it cannot withstand a lot of traction strength before reaching its breaking point.

Medium carbon steel has a carbon content of 0.25 to 0.45% and, unlike mild steel, has a good balance between strength and ductility. It is wear resistant and used for the production of big components requiring a combination of strength, toughness and wear resistance.

High carbon steel contains 0.45 to 1.0% carbon, meaning it has a higher hardness than other types but is very difficult to weld because of the decrease in ductility.

Finally, ultra-high carbon steel contains 1.0 to 2.1% carbon which makes them very hard and therefore not suitable for construction.

In addition to all these characteristics, it is important to note that the carbon content of a metal influences the corrosion it will undergo, making carbon steel more susceptible to corrosion than stainless steel (De Baere et al., 2017).

Different alloys will be chosen depending on their use, which is why the naming of construction steel is also made according to its purpose. Their name can thus begin with an S, for Structure, or with E, for Engines. The former type is dedicated to a general use, while the latter is particularly used for mechanical engineering. This letter is followed by the yield strength in megapascal (MPa), a figure representing the stress at which the material starts to deform plastically, i.e. permanently. This value is of great importance when selecting a structural steel, as it gives an indication of the stiffness, deformability and weldability of a steel. In the steel denomination, this yield strength is directly followed by an index (JR, J0, J2, J3, ...) giving an indication of the quality of the steel and its risk of crack propagation and, consequently, of failure. It is the result Charpy impact test, carried out at several temperatures in order to measure the toughness of the steel, i.e. its resistance before breaking and its resistance to shocks. A summary of this denomination can be found in Table 2.

**Table 2 Charpy test indicator**

*The letter J represents the energy at which the Charpy test was conducted. The second figure of the index represents the temperature at which the test was carried, R meaning room temperature.*

(Meyers & Chawla, 1999)

Energy required for rupture (Joules)		Temperature (°C)
27J	40J	
JR	KR	+20 (room temperature)
J0	K0	0
J2	K2	-20
J3	K3	-30
J4	K4	-40

### 3.1.1 Difference in corrosion rate between carbon and stainless steels

As a general rule, stainless steels are more resistant to corrosion because they contain a higher percentage of chromium (minimum 10.5%) than carbon steel (Ans, 2017). When the chromium in the metal is exposed to the ambient air or any oxidising environment, a reaction occurs, and a thin layer spontaneously forms on the surface of the metal. This layer, called the passive layer or passive film, is self-repairing and acts as a protection for the stainless steel (Figure 5). It blocks the diffusion of oxygen to the surface and also prevents oxidation from spreading through the metal (Steel Construction Institute (Great Britain), 2017).

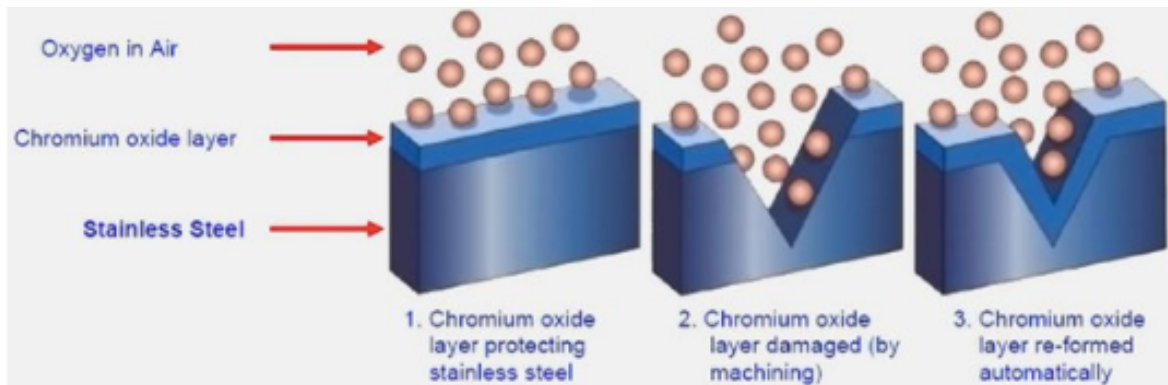


**Figure 5 Self reparation of stainless steel**

(Nguyen Le, 2017)

Carbon steel, on the other hand, does not contain chromium and is therefore not protected against corrosion. In order to slow down the rate of corrosion of this type of metal, coating or barrier layers should be added. This process is called artificial passivation and is obviously less effective than self-passivation because barrier layers suffer adherence decay and tend to degrade over time, as shown in Figure 6.

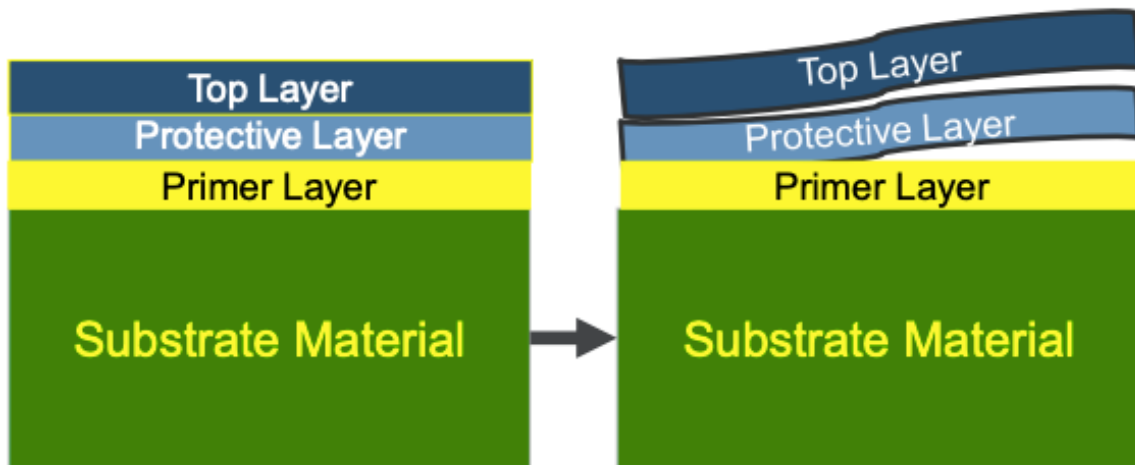


**Figure 6** *Degrading of coating layers over time*

(www.worldstainless.org)

The difference in corrosion resistance between stainless and carbon steels can be seen in Figure 7, which represents the corrosion rate as a function of the percentage of chromium present in the metal. As soon as a 10.5% chromium concentration is reached, or in other words when the distinction is made between oxidizable and stainless steel, the curve becomes constant and the corrosion rate practically negligible.

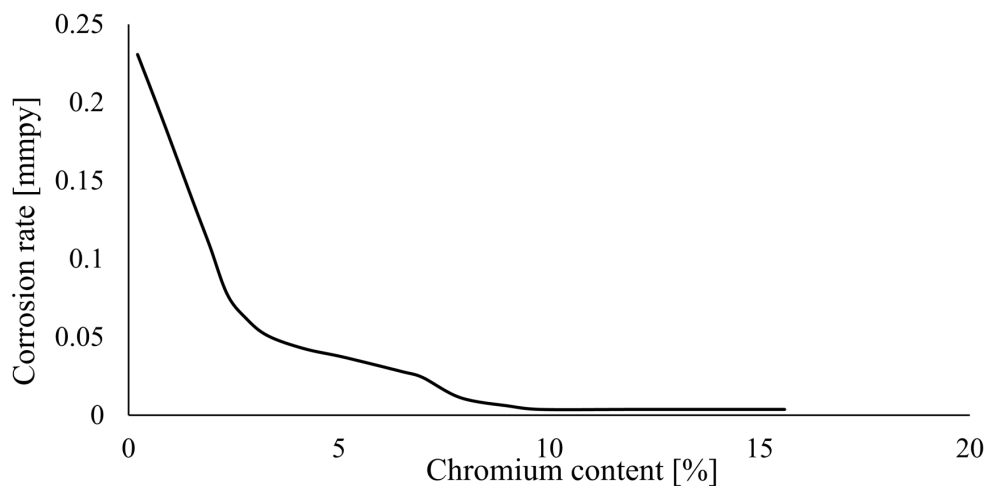


**Figure 7** *Corrosion rate as a function of chromium percentage*

(Karabulut, 2021)

### 3.2 Description of the tested specimens

**Grade A steel** is a type of carbon steel often used in the construction of ship hulls. The exact type used is S235JR. It is the most common type of construction steel, with a yield strength of 235 MPa and a JR quality, meaning that it has a guaranteed minimum breaking energy of 27J at room temperature. The exact chemical composition of this steel type (Table 3) shows that this alloy contains 0.140% carbon and can therefore be considered a mild steel. Furthermore, its low chromium content (0.023%) proves that it is not a stainless steel and that it will therefore not be resistant to corrosion.

*Table 3 Chemical composition of S235JR carbon steel  
Values are given in molar fraction*

(<https://www.azom.com>)

C	Si	Mn	P	S	N	Cr	Cu	Mo	Al	Ni
0.140	0.003	0.696	0.017	0.010	0.0030	0.023	0.010	0.02	0.067	0.015

The second type of carbon steel used is **S355J2+N**, a structural steel with a minimal yield strength of 355 MPa and a J2 quality, meaning that it has a guaranteed minimum breaking energy of 27J at -20°C. Two batches of alloys with slightly different compositions are used. Although there is a small difference in the composition of these steels (Table 4), it can be considered negligible for the purpose of this experiment. The two sets of coupons are therefore expected to corrode in a similar way.

*Table 4 Chemical composition of S355J2 carbon steel*

(<https://www.azom.com>)

	C	Si	Mn	P	S	B	Cr	Cu	Mo	Al	Nb
Batch 1	0.174	0.016	1.500	0.014	0.0070	0.0002	0.034	0.020	0.004	0.044	0.001
Batch 2	0.177	0.011	1.530	0.015	0.0100	0.0002	0.041	0.016	0.005	0.033	0.001

**316L stainless steel**, or 1.4404 stainless steel as per American denomination, is a type of steel that has excellent corrosion resistance (Outokumpu, 2020). It is often used for marine purposes but can be subject to pitting or crevice corrosion when exposed to warm sea water. It is a molybdenum-alloyed austenitic steel belonging to CrNiMo standard (the exact type being CrNiMo 17-12-2).

As explained in paragraph 3.1, a steel containing more than 10% chromium is considered stainless. 316L contains between 16.5 and 18.5 percent of chromium by mass (Table 5) and therefore falls directly into this category.

One of its characteristics is its low carbon content (<0.030% by mass), which makes it very weldable. Another important feature, and probably its most important feature, is that it contains a high level of molybdenum (2.00 to 2.50% by mass), which makes it more resistant to corrosion than some other types of steel (Outokumpu, 2020).

*Table 5 Composition of 316L stainless steel in percentage by mass*

(<https://www.lksteelpipe.com>)

C	Si	Mn	P	S	N	Cr	Cu	Mo	Nb	Ni	Others
<0.030	<1.00	<2.00	0.045	≤0.015	≤0.11	16.5 to 18.5		2.00 to 2.50		10.0 to 13.0	

The mechanical properties of 316L stainless steel can be found in Table 6.

*Table 6 Mechanical properties of 316L stainless steel*

(<https://bssa.org.uk>)

Property	Max. thickness	0.2% proof strength (R <sub>p0.2</sub> )	1% proof strength (R <sub>p1.0</sub> )	Tensile strength (R <sub>m</sub> )	Min. elongation after fracture (<3mm thick)	Min. elongation after fracture (≥3mm thick)
<b>Unit</b>	mm	MPa	MPa	MPa	%	%
<b>Value</b>	8	240	270	530 to 680	40	40

### 3.3 Forms of corrosion to be expected on each specimen

As mentioned in paragraph 1.4, there are several forms of corrosion. Because of their different composition, and mainly because one has a natural passive layer and the other has not, stainless and carbon steels will not corrode in the same way.

The Steel Construction Institute (2017) explains that, although uniform corrosion is very unlikely to occur on stainless steel, it does not mean that it is immune to every form of corrosion. Indeed, pitting or crevice corrosion may occur on stainless steel when its passive film is exposed to certain chemical species/certain aggressive environments.

Pitting is a form of corrosion which occurs at specific places on the metal surface. Once it has started, it is aggravated by the galvanic current between the pit and the rest of the metal. In the case of stainless steel, it results from the local breakdown of the passive film. Most of the time, it happens because of chloride ions which attack the metal, but of course it is also enhanced by other environment related factors such as corrosive pollutants, temperature, acidity, presence of oxygen and content of oxidizing agents.

As for crevice corrosion, it occurs in oxygen-poor areas which become the anode of a corrosion cell.

The resistance of the steel to both forms of corrosion is directly related to its composition. An increase of alloying elements such as chromium, molybdenum and nitrogen implies an increase in resistance of the metal (Di Schino, 2020; Nickel Development Institute & Specialty Steel Institute of North America, n.d.). It is therefore obvious that it is important to choose the correct steel grade for its intended application.

As for carbon steel, due to its absence of a natural protective layer, it is expected to corrode in a more general way but can also show signs of pitting corrosion (Kefarge, Werkneh, Tegegne, & Gashaw, 2014).

## 4 Measuring equipment

As the water purification system used belongs to the KULeuven and is used for other projects, changing any parameters to see their effect on corrosion was not allowed. However, the parameters currently present in the reactors can be monitored. The evolution of these parameters and the corrosion rate were measured with two sensors, respectively an environmental probe and an LPR probe. The data were collected at 30-minute intervals.

### 4.1 The Aquaread 800 environmental probe

#### 4.1.1 General description of the probe

The type used is an AquaRead 800 probe (Figure 8) sold by Eijkelkamp (The Netherlands). It is equipped with a three-metre long cable and a USB cable, and is connected to a portable GPS with IP67 protection for outdoor use. Thanks to the GPS it is possible to know the exact geographical position of all measured data. The probe is made of aluminium for marine application, which allows it to be used in fresh water, seawater or even wastewater.



**Figure 8** *Multiparameter AP-800 set*

(Eijkelkamp Soil & Water, 2017)

#### 4.1.2 Parameters measured by the probe

This probe is capable of measuring several parameters, namely temperature (in °C), dissolved oxygen concentration (in mg/L), salinity (in Practical Salinity Units (PSU)), chloride concentration (in mg/L), conductivity (in  $\mu\text{S}/\text{cm}$ ), depth (in m), TDS (in mg/L), pH, redox potential (in mV) and turbidity (in Nephelometric Turbidity Units (NTU)). Table 7 lists the parameters that are of interest for this thesis and for each of them it is indicated whether they are controllable or not, as well as the available range and the range on which the experiment will focus.

As mentioned in paragraph 2.1, the temperature of the system is 5°C for two of the bioreactors and room temperature for the other bioreactors, which explains the choice of range of 4°C up to 30°C. The pH being maintained around a neutral value in all four reactors, a range of interest of 6 to 8 has been chosen in order to allow for a possible margin of variation.

**Table 7** *Parameters measured by the environmental probe*

(Eijkelkamp Soil & Water, 2017)

	<b>Measurable?</b>	<b>Possible range</b>	<b>Range of interest</b>
<b>Temperature (°C)</b>	Yes	(-5) – (+50)	4 - 30
<b>pH</b>	Yes	0 - 14	6 - 8
<b>Dissolved oxygen (mg/L)</b>	Yes	0 - 50	2 - 8
<b>Salinity (PSU)</b>	Yes	0 - 70	10 – 35k mg/L
<b>Conductivity (<math>\mu\text{S}/\text{cm}</math>)</b>	Yes	0 - 200	1 - 100
<b>ORP (mV)</b>	Yes	$\pm 2000$	
<b>Turbidity (NTU)</b>	Yes	0 - 3000	
<b>Chloride (mg/L)</b>	No	0 - 20	10 – 20k

As explained in section 1.3, some of these factors may be interdependent. In order to properly understand their influence on corrosion rate, it is wise to focus on one factor at a time. By varying a single parameter, it will be possible to study its impact not only on the rate and speed of corrosion, but also on the other parameters that will inevitably also influence the corrosiveness of the environment. Attempting to vary several parameters at the same time would not allow an understanding of the individual behaviour of each and would therefore lead to a less precise study of the environment in question.

## 4.2 LPR probe

### 4.2.1 General description of the probe

The second sensor used is an LPR 6112 probe developed by Cosasco to measure linear polarisation resistance. The probe is made of epoxy and has two electrodes mounted at its end by threaded studs.

### 4.2.2 Parameters measured by the probe

Unlike the environmental probe, the LPR probe does not measure parameters specific to the environment in which the metal is placed, but directly measures the rate of corrosion and the qualitative pitting tendency of the metal when in an electrolyte solution.

This is measured using a technique called Linear Polarisation Resistance, from which the probe takes its name.

In this system, the probe interacts with the electrochemical corrosion mechanism to determine the rate at which metal ions pass into the electrolyte solution, i.e. the rate at which the metal corrodes (Mittemeijer, 2015; Speight, 2014).

Two electrodes are used (working electrode and counter electrode), and between those electrodes a small potential is created by a transmitter applying a voltage every 30 minutes. As a way of resisting to this voltage, the electrodes produce a current which responds to the same anodic and cathodic reactions that control the corrosion current.

If the electrodes corrode rapidly as the metal ions pass through the solution, the low potential applied between the electrodes is sufficient to produce a large current or low polarisation resistance. Conversely, if the electrodes corrode at a low rate, a small potential between the two electrodes will result in only a small current, or a large polarisation resistance. Thus, a

large current corresponds to a high corrosion rate, while a small current corresponds to a low corrosion rate.

#### 4.2.3 Positioning of the probe in the water purification system

In order to get the most representative readings possible, the probes should be installed where the corrosion rate is likely to be the highest. Also, if the probe is used to measure corrosion in a flowing environment (which is the case in this experiment), it is advisable to position the probe where the flow velocity exceeds 0.3 m/s.

It is important to align the electrodes with the flow in order to get reliable measurements, otherwise one electrode could shield the other from full flow. The orientation of the probes should be as shown in Figure 9.

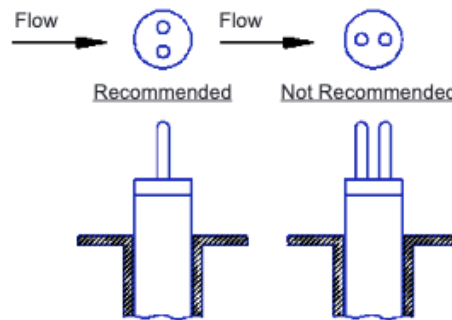


**Figure 9** *Probe orientation relative to flow*

(<https://www.cosasco.com>)

In order to achieve this alignment, the probe was mounted on a holding rack which also contains the metal coupons. This holding rack (Figure 10) was then placed in the anoxic reactor kept at room temperature.

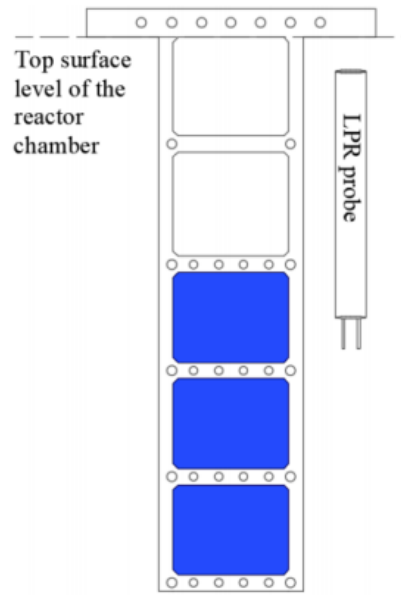


*Figure 10 Positioning of the LPR probe on the holding rack*

## 5 Experimental process

### 5.1 Placing of the metal coupons in the bioreactor

The measurements were taken on metal plates of type S235JR Grade A steel, placed in the water purification system on 23/03/2021.

For this purpose, 12 metal coupons were attached to a holding rack placed in the anoxic bioreactor working at room temperature. These coupons were first weighed and then attached to the plastic frame in such a way as not to touch each other in order to have as much free surface as possible (Figure 11).

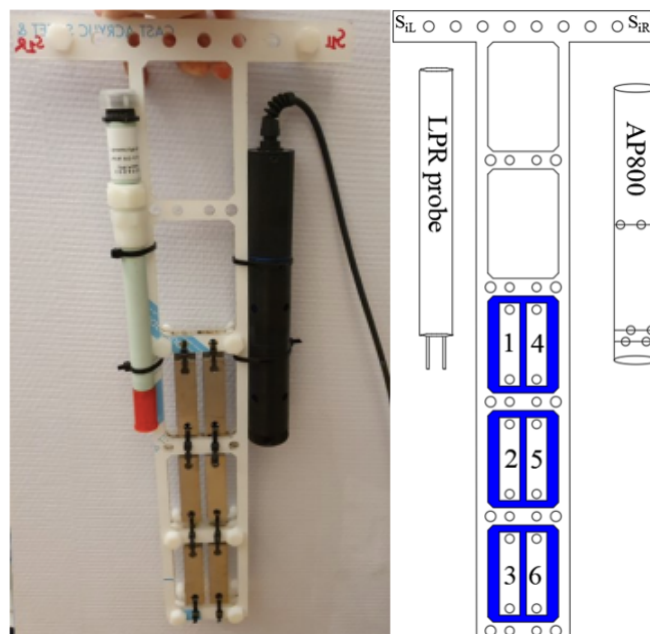


*Figure 11 Holding rack for metal coupons*

In order to remember which mass corresponds to which coupon, a nomenclature system has been developed. The holding rack consists of two faces, one named S1 and the second S2. Each of these faces is divided into two sides: the right side named R, the left side L. There is therefore a total of four parts (S1R, S1L, S2R, S2L) on which coupons are attached. These coupons are numbered from top to bottom.

The weight of each of these coupons can be found in Table 8, in which the same nomenclature system is used to facilitate visual understanding of the system. The values shown in Table 8 include decimals down to the nanogram, which may seem surprising but can be explained by the fact that the initial weighed masses were multiplied by a correction

factor to account for the loss of material due to the cleaning of the coupons with a chemical (Ferrer & Kelly, 2001).

*Table 8 Weight of coupons before first immersion*

<b>S1L</b>		<b>S1R</b>	
<b>1</b>	35.94397298 g	<b>4</b>	35.47573096 g
<b>2</b>	35.70175471 g	<b>5</b>	35.99155693 g
<b>3</b>	36.07382917 g	<b>6</b>	36.01964745 g
<b>S2L</b>		<b>S2R</b>	
<b>1</b>	35.8976886 g	<b>4</b>	35.51461784 g
<b>2</b>	36.08622499 g	<b>5</b>	35.54580732 g
<b>3</b>	35.5503058 g	<b>6</b>	35.37406526 g

## 5.2 Preparation of the necessary tools for the statistical analysis

In order to best interpret all the data collected by the probes during the experiment, several graphs were drawn, among others by means of an R script.

The first step in writing this script was to import the packages that could be useful for the realisation of the various desired graphs (Figure 12).

The “readxl” package allows to read the Excel document in which all the data collected by the probes have been transcribed. The “plyr” package allows to divide, apply and combine data. The scales package allows aesthetic modifications of the visualization and function of the graph axes. The “usethis” package automates functions that would otherwise have to be done by hand, thus avoiding repetitive coding. “ggplot2” and “ggbiplot” are the packages that allow the graphs to be created, and the “GGally” and “cowplot” packages are extensions to ggplot2 that allow certain functions to be added to facilitate the combination of geometric objects with transformed data, or to align plots into complex figures and to annotate those plots. Similarly, “tggpubr” is an extension to ggplot2 that allows to format the plots before sending them to publication. The “gridExtra” package allows several graphs to be displayed on a single page.

After importing the necessary packages from the library, the Excel workbook containing all the data to be used was imported and cleaned to remove incomplete data sets (Figure 12).

```

#import analysis packages
library(readxl)
library(plyr)
library(scales)
library(grid)
library(usethis)
library(devtools)
library(ggplot2)
library(ggbplot)
library(GGally)
library(cowplot)
library(ggpubr)
library(gridExtra)

#import and check data
corrosiondataKUL <- read_excel("corrosiondataKUL.xlsx",
                             sheet = "final")

View(corrosiondataKUL)
corrdata<-corrosiondataKUL #make working copy of full dataset
corrdata <- na.omit(corrdata) #remove incomplete datasets
head(corrdata) #check if data were properly imported

```

*Figure 12 R Script Part 1 - importing packages and data*

The second step was to produce simple graphs allowing the visualisation of each environmental parameter as a function of time. To do this, the “geom\_point” function of ggplot2, which allows the creation of scatterplots, was used (Figure 13).

```

# GENERAL ANALYSIS
# =====
tp1 <- ggplot(corrdata, aes(Day, Temperature)) + geom_point() +
  xlab("Time (days)") + ylab("Temperature (°C)")
tp2 <- ggplot(corrdata, aes(Day, DO_mgperL)) + geom_point() +
  xlab("Time (days)") + ylab("Dissolved oxygen (mg/L)")
tp3 <- ggplot(corrdata, aes(Day, Conductivity)) + geom_point() +
  xlab("Time (days)") + ylab("Conductivity (µS/cm)")
tp4 <- ggplot(corrdata, aes(Day, pH)) + geom_point() +
  xlab("Time (days)") + ylab("pH")
tp5 <- ggplot(corrdata, aes(Day, ORP)) + geom_point() +
  xlab("Time (days)") + ylab("Oxidoreduction potential (mV)")
tp6 <- ggplot(corrdata, aes(Day, Turbidity)) + geom_point() +
  xlab("Time (days)") + ylab("Turbidity (NTU)")
tp7 <- ggplot(corrdata, aes(Day, Salinity)) + geom_point() +
  xlab("Time (days)") + ylab("Salinity (given as PSU)")
tp8 <- ggplot(corrdata, aes(Day, Corrosionrate_mmPY)) + geom_point() +
  xlab("Time (days)") + ylab("Corrosion rate (mm/y)")

ggarrange(tp1, tp2, tp3, tp4, tp5, tp6, tp7, tp8, labels
          = c("A", "B", "C", "D", "E", "F", "G", "H"), ncol = 2, nrow = 4)

```

*Figure 13 R Script Part 2 - General analysis*

In order to study the quartile distribution for each variable, boxplots were made using the “geom\_boxplot” function of ggplot2 (Figure 14). Then, pairs were made in order to compare two variables with each other.

```
# BOXPLOTS AND CORRELATIONS
# =====
labels <- c("Temperature (°C)", "Dissolved oxygen (mg/L)",
           "Conductivity (µS/cm)", "pH",
           "ORP (mV)", "Turbidity (NTU)",
           "Salinity (given as PSU)", "Corrosion rate (mm/y)")
bp1 <- ggplot(corrdata, aes(x = "", y = Temperature)) + geom_boxplot() +
  ggtitle(labels[1]) + theme(axis.title.x = element_blank())
bp2 <- ggplot(corrdata, aes(x = "", y = DO_mgperL)) + geom_boxplot() +
  ggtitle(labels[2]) + theme(axis.title.x = element_blank())
bp3 <- ggplot(corrdata, aes(x = "", y = Conductivity)) + geom_boxplot() +
  ggtitle(labels[3]) + theme(axis.title.x = element_blank())
bp4 <- ggplot(corrdata, aes(x = "", y = pH)) + geom_boxplot() +
  ggtitle(labels[4]) + theme(axis.title.x = element_blank())
bp5 <- ggplot(corrdata, aes(x = "", y = ORP)) + geom_boxplot() +
  ggtitle(labels[5]) + theme(axis.title.x = element_blank())
bp6 <- ggplot(corrdata, aes(x = "", y = Turbidity)) + geom_boxplot() +
  ggtitle(labels[6]) + theme(axis.title.x = element_blank())
bp7 <- ggplot(corrdata, aes(x = "", y = Salinity)) + geom_boxplot() +
  ggtitle(labels[7]) + theme(axis.title.x = element_blank())
bp8 <- ggplot(corrdata, aes(x = "", y = Corrosionrate_mmPY)) + geom_boxplot() +
  ggtitle(labels[8]) + theme(axis.title.x = element_blank())
ggarrange(bp1, bp2, bp3, bp4, bp5, bp6, bp7, bp8,
          labels = c("A", "B", "C", "D", "E", "F", "G", "H"),
          ncol = 4, nrow = 2)

# pairs(corrdata[,3:10]) #original pairwise plot
ggpairs(corrdata[,3:10],
        columnLabels = c("Temperature (°C)", "Dissolved oxygen (mg/L)",
                        "Conductivity (µS/cm)", "pH",
                        "ORP (mV)", "Turbidity (NTU)",
                        "Salinity (given as PSU)",
                        "Corrosion rate (mm/y)"))
```

*Figure 14 R Script Part 3 - Boxplots and correlations*

The final step in writing this script was to prepare all the necessary data for a Principal Components Analysis, which will be discussed in detail in paragraph 6.2.2. To do so, the “prcomp”, “ggscreeplot” and “ggbiplot” functions were used (Figure 15)

```

# PRINCIPAL COMPONENT ANALYSIS - BIPLLOT
# =====
#           CALCULATIONS PCA
#           -----
corrdata2.pca <- prcomp(corrdata[,3:9], scale. = TRUE, center = TRUE)

#           SCREEN PLOT
#           -----
print(ggscreeplot(corrdata2.pca) + ggtitle("Screeplot"))

#           BIPLOTS
#           -----
corr.level <- as.matrix(corrdata[,10])
day <- as.matrix(corrdata[,2])

g2 <- ggbiplot(corrdata2.pca, choices=c(1,2), obs.scale = 0.5, var.scale = 1,
              circle = TRUE, varname.size = 4) +
  theme(legend.direction = 'horizontal', legend.position = 'bottom') +
  ggtitle("Biplot - Corrosion rates - PC1 & 2") +
  geom_point(aes(colour = corr.level))+
  scale_colour_gradient(
    low = "black",
    high = "yellow"
  )
)
g2$layers <- c(g2$layers[[3]], g2$layers[[5]], g2$layers[[2]], g2$layers[[4]],
              g2$layers[[1]]) print(g2)

g3 <- ggbiplot(corrdata2.pca, choices=c(1,3), obs.scale = 0.5, var.scale = 1,
              circle = TRUE, varname.size = 4) +
  theme(legend.direction = 'horizontal', legend.position = 'bottom') +
  ggtitle("Biplot - Corrosion rates - PC1 & 3") +
  geom_point(aes(colour = corr.level))+
  scale_colour_gradient(
    low = "black",
    high = "yellow"
  )
)
g3$layers <- c(g3$layers[[3]], g3$layers[[5]], g3$layers[[2]], g3$layers[[4]],
              g3$layers[[1]]) print(g3)

g4 <- ggbiplot(corrdata2.pca, choices=c(2,3), obs.scale = 0.5, var.scale = 1,
              circle = TRUE, varname.size = 4) +
  theme(legend.direction = 'horizontal', legend.position = 'bottom') +
  ggtitle("Biplot - Corrosion rates - PC2 & 3") +
  geom_point(aes(colour = corr.level))+
  scale_colour_gradient(
    low = "black",
    high = "yellow"
  )
)
g4$layers <- c(g4$layers[[3]], g4$layers[[5]], g4$layers[[2]], g4$layers[[4]],
              g4$layers[[1]]) print(g4)

g5 <- ggbiplot(corrdata2.pca, choices=c(1,2), obs.scale = 0.5, var.scale = 1,
              circle = TRUE, varname.size = 4) +
  theme(legend.direction = 'horizontal', legend.position = 'bottom') +
  ggtitle("Biplot - Corrosion rates - PC1 & 2") +
  geom_point(aes(colour = day))+
  scale_colour_gradient(
    low = "black",
    high = "green"
  )
)
g5$layers <- c(g5$layers[[3]], g5$layers[[5]], g5$layers[[2]], g5$layers[[4]],
              g5$layers[[1]]) print(g5)

```

*Figure 15 R Script Part 4 - Principal Components Analysis*

## 6 Results and discussions

### 6.1 Description of the environmental sensory output

#### 6.1.1 Temperature

The temperature of the system was measured continuously between 01/04/2021 and 29/06/2021. These measurements vary between 15 and 30°C (Figure 16), which is explained by the fact that they were taken in the reactor maintained at room temperature. From May onwards, higher temperatures can be observed than in the previous months, which is quite logical as the outside temperature increases due to the change of season. At the beginning of July, however, there is a sudden drop in temperature compared to the last week of June, which again can be explained by the weather conditions of that period.

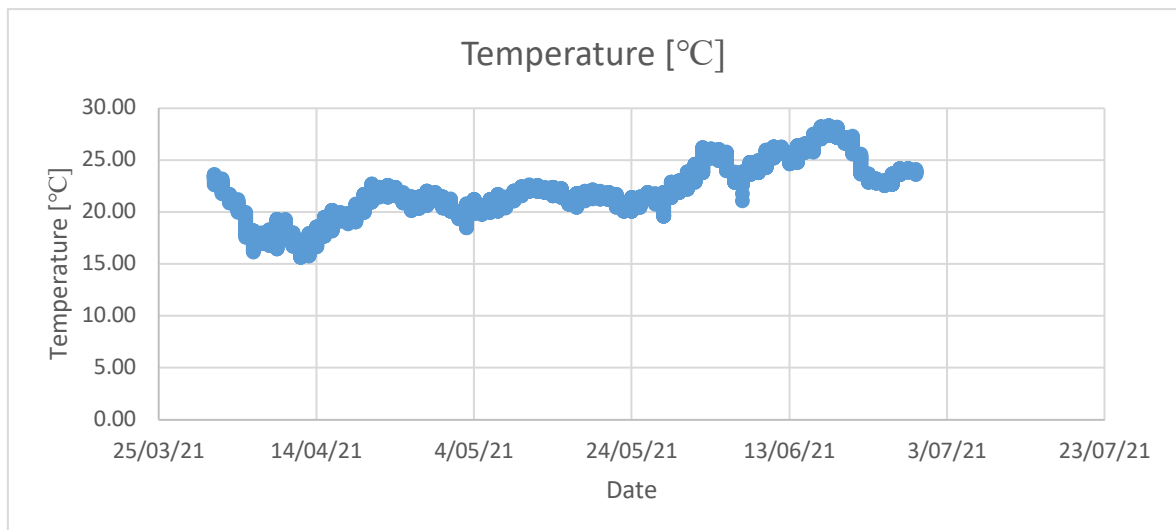


*Figure 16 Temperature (°C) measured between 01/04/2021 and 29/06/2021*

In terms of daily variation, there is a slight drop in temperature at night and a rise during the day (Figure 17). As the laboratory in which the reactors are located is directly exposed to the sun, it is normal to have higher temperatures during daytime. However, in general, there is no variation within days but there is one between days.

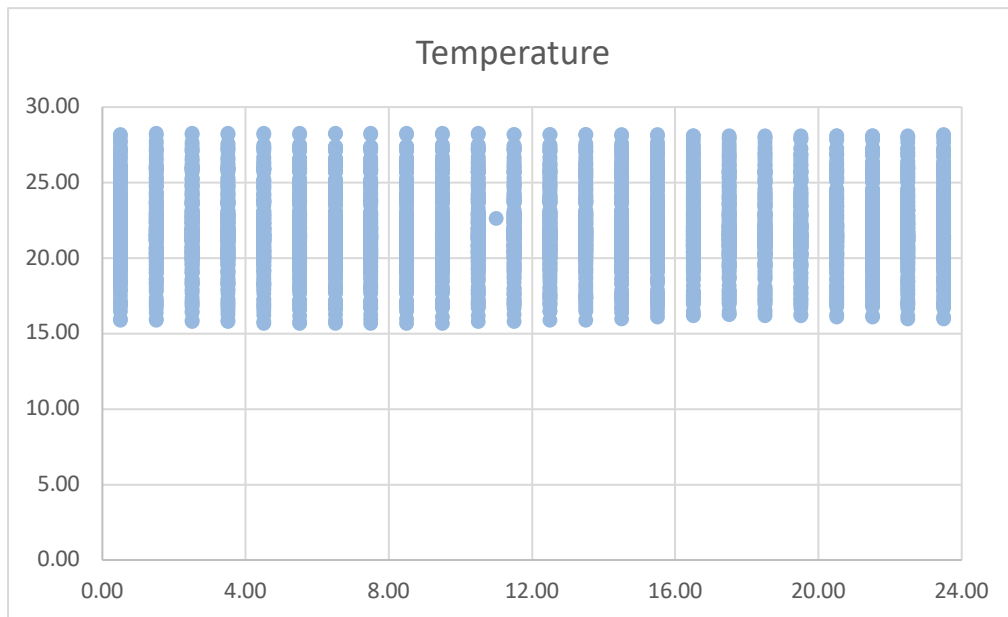


*Figure 17 Daily temperature variation (°C) for period 01/04/2021 to 29/06/2021*

In order to facilitate the reading of these values, it is possible to represent them as a boxplot (Figure 18). In doing so, it can be seen that there are as many values above 21.63°C as below this temperature. 50% of the measured temperatures are between 20.40°C and 23.70°C. However, there are minima that reach up to 15.70°C and maxima that reach up to 28.30°C.

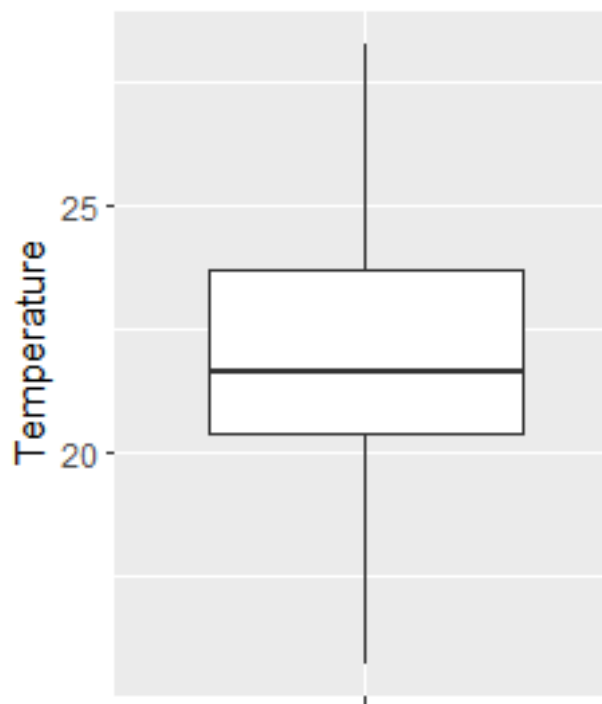


*Figure 18 Measured values of temperature (°C) – boxplot*

### 6.1.2 Conductivity

The conductivity values measured between 01/04/2021 and 29/06/2021 increase with time. Indeed, the last measured value (1748  $\mu\text{S}/\text{cm}$ ) is almost the double of the first value (888  $\mu\text{S}/\text{cm}$ ), measured only a few months before (Figure 19).

This conductivity represents the capacity of the system to conduct heat and electricity. As mentioned in point 1.3, if the conductivity increases, so does the corrosion. From the measured values, it can be assumed that corrosion also increased between the period of 01/04/2021 to 29/06/2021.

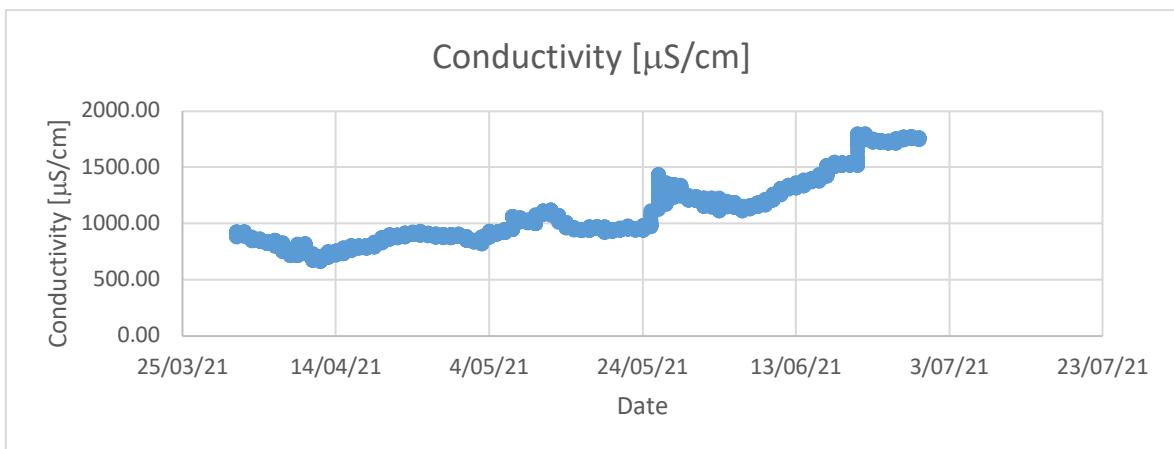


*Figure 19 Conductivity ( $\mu\text{S}/\text{cm}$ ) measured between 01/04/2021 and 29/06/2021*

As for the daily variation, the conductivity stays quite constant throughout the day. Only fluctuations over several days can be observed (Figure 20).

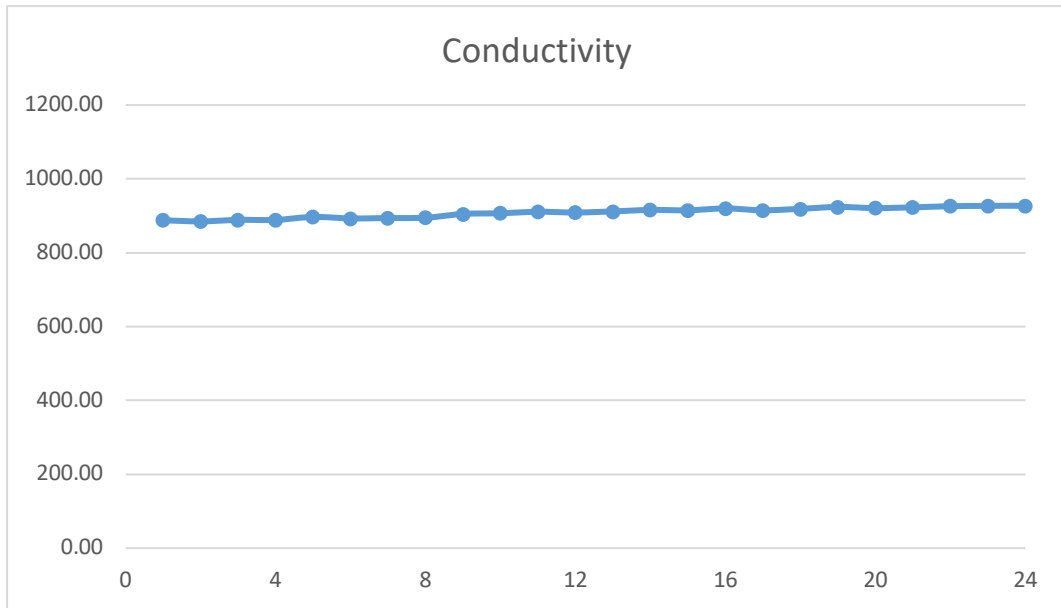


*Figure 20 Daily variation of conductivity ( $\mu\text{S/cm}$ ) for period 01/04/2021 to 29/06/2021*

Representing this as a boxplot (Figure 21), it appears that half of the measured values for conductivity are between 883  $\mu\text{S/cm}$  and 1239  $\mu\text{S/cm}$ , with a median value of 967  $\mu\text{S/cm}$ . Some extreme values can reach a minimum of 668  $\mu\text{S/cm}$  and a maximum of 1801  $\mu\text{S/cm}$ .

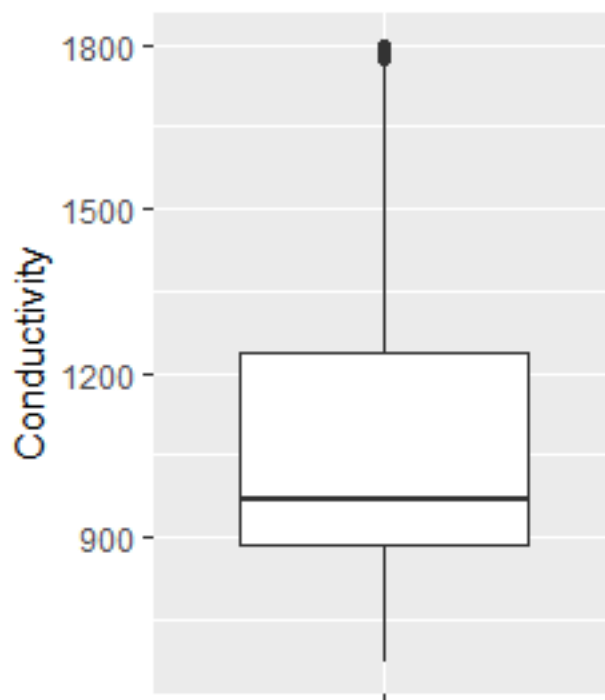


*Figure 21 Measured values of conductivity ( $\mu\text{S/cm}$ ) – boxplot*

### 6.1.3 Salinity

The salinity values observed between 01/04/2021 and 29/06/2021 show an increase with time, ranging from 0.39 to 0.91 PSU (Figure 22).

These values are expressed in Practical Salinity Units but it should be emphasized that, strictly speaking, practical salinities do not have units. PSU is therefore a relative unit which is only used as a way of qualifying the numerical values obtained for salinity. In order to have a better understanding of what these values represent, a relation can be made between salinity and the mass fraction of dissolved matter, expressed as grams of solute per kilogram of water. Salinity is about 0.5% smaller than this mass fraction (Pawlowicz, 2013).

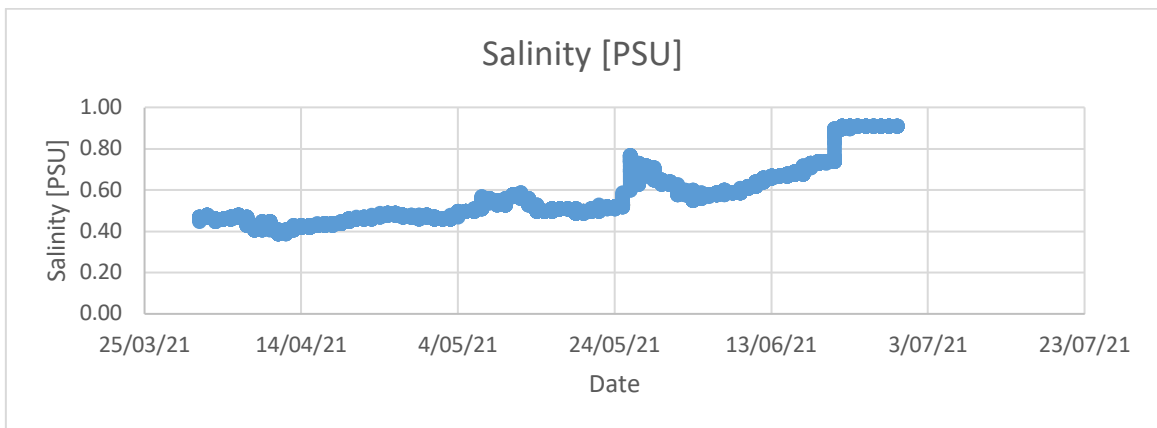


*Figure 22 Salinity (PSU) measured between 01/04/2021 and 29/06/2021*

Just as the values measured for conductivity, those of salinity increase stay quite constant throughout the day (Figure 23).

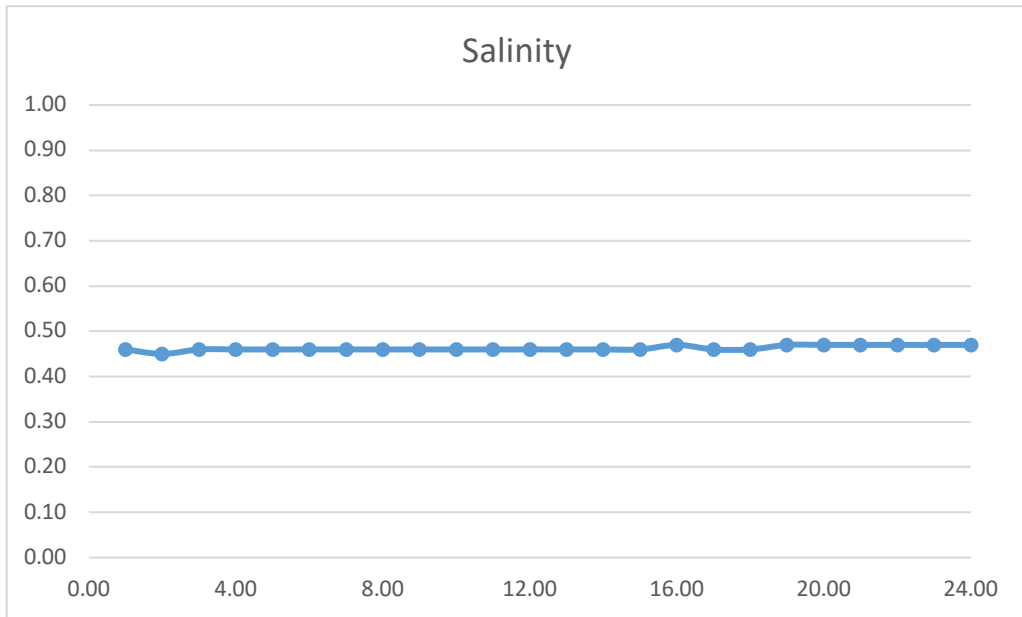


*Figure 23 Daily variation of salinity (PSU) for period 01/04/2021 to 29/06/2021*

Representing this as a boxplot (Figure 24) it appears that half of the measured values for salinity are between 0.47 and 0.64 PSU, with a median value of 0.52 PSU. Some extreme values can reach a minimum of 0.39 PSU and a maximum of 0.91 PSU.

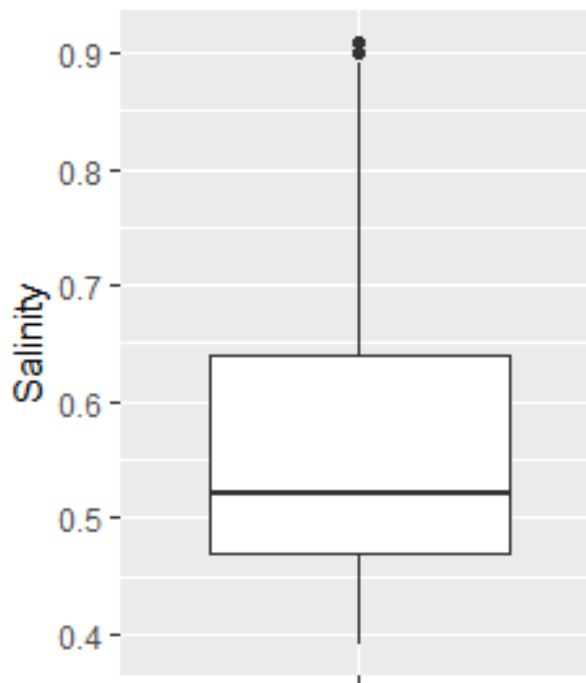


*Figure 24 Measured values of salinity (PSU) – boxplot*

#### 6.1.4 Dissolved oxygen

The dissolved oxygen values measured between 01/04/2021 and 29/06/2021 (Figure 25) show some peaks but remain close to zero overall. These near-zero values can be explained by the fact that the probe was placed in a reactor in anoxic condition. The few peaks correspond to the moments when the probe was moved and to certain moments when the biocarriers were blocked in the system. Oxygen is introduced into the reactor to set the carriers in motion, and this oxygen is then absorbed by the bacteria. The blockage of the carriers reduced the absorption by the bacteria, causing oxygen to accumulate in the reactor at certain times.

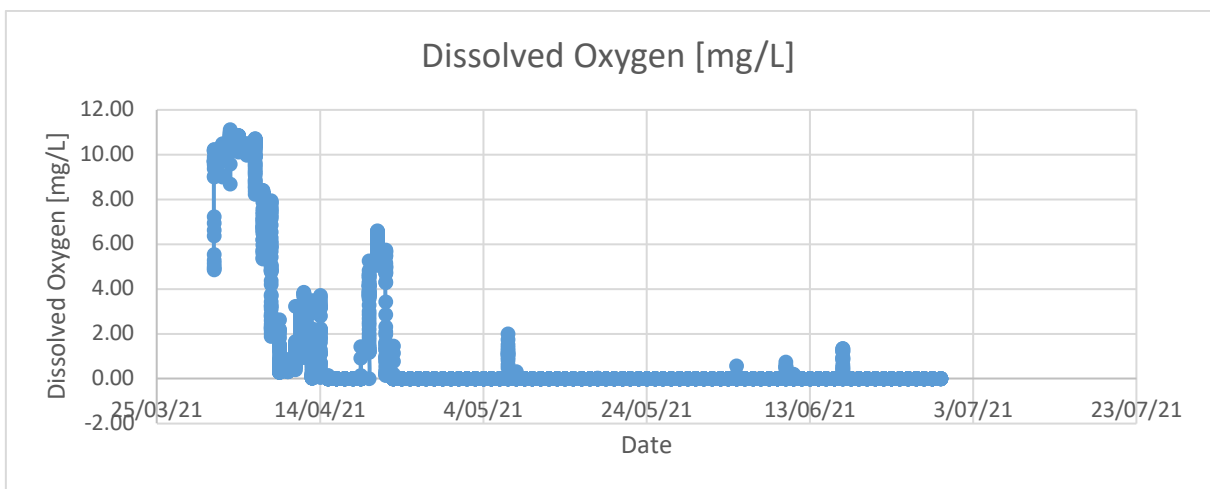


*Figure 25 Dissolved oxygen (mg/L) measured between 01/04/2021 and 29/06/2021*

The amount of dissolved oxygen seems to double throughout the day, going from 60 mg/L to about 120 mg/L (Figure 26).

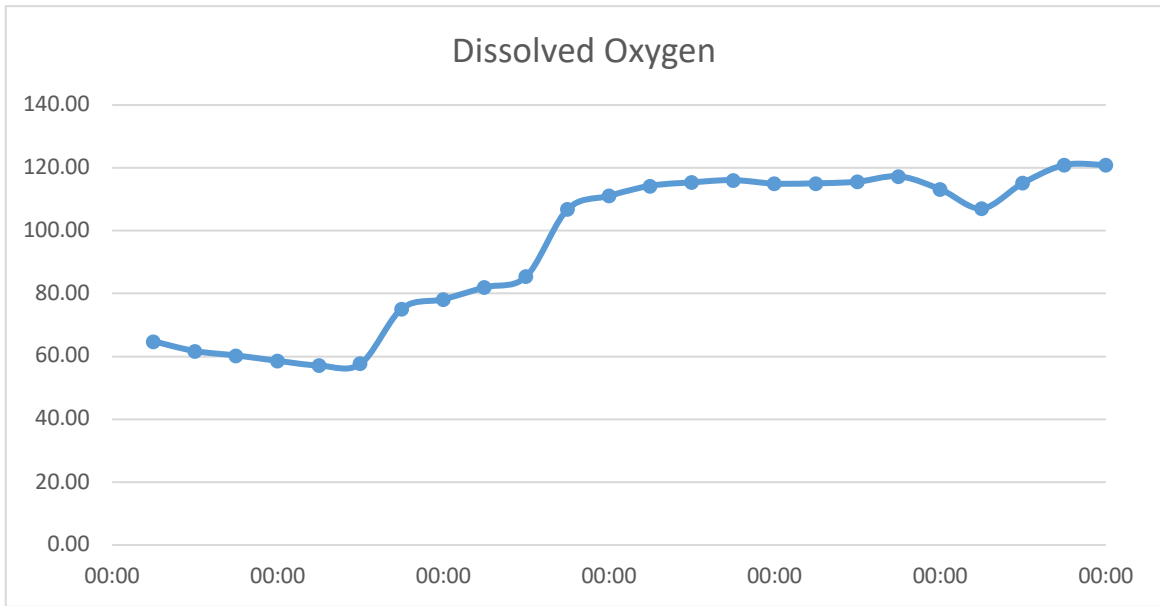


*Figure 26 Daily variation in dissolved oxygen content (mg/L) for period 01/04/2021 to 29/06/2021*

The study of the quartiles of this variable (Figure 27) clearly shows the anoxic condition of the environment in which the tests were carried out, since most of the values measured are zero.

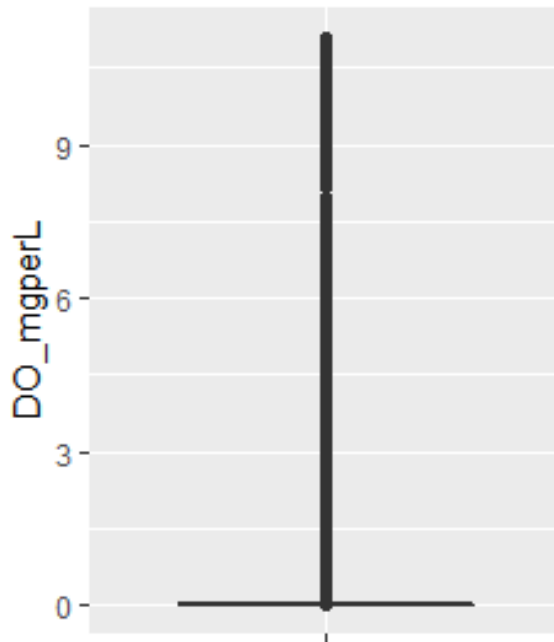


*Figure 27 Measured values of dissolved oxygen concentration (mg/L) – boxplot*

### 6.1.5 pH

As the pH of the system is deliberately kept at a neutral level, there is not much variation to be observed in the measured values (Figure 28).

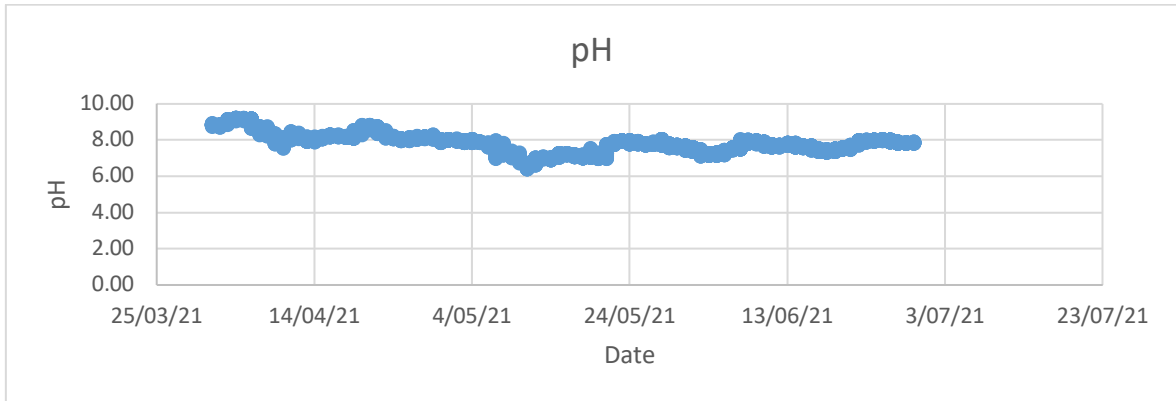


*Figure 28 pH values measured between 01/04/2021 and 29/06/2021*

This maintenance of the pH around a neutral value can be represented in the form of a boxplot (Figure 29), in which it can be seen that there are as many measured values above 7.86 as there are values below this pH. 50% of measured pH values are between 7.50 and 8.11, with minima reaching a value of 6.42 and maxima up to 9.22.

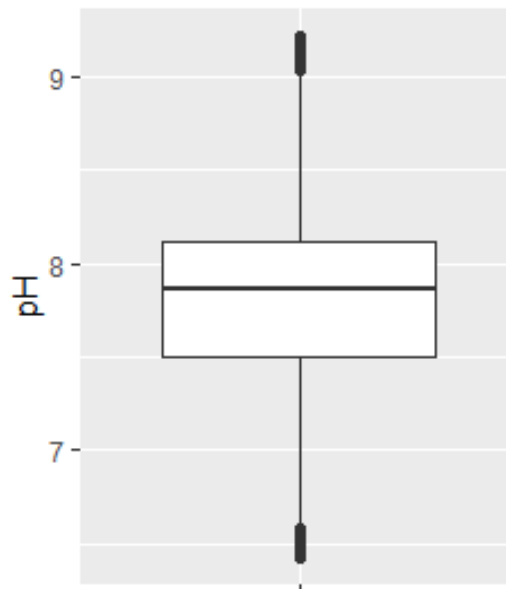


*Figure 29 Measured values of pH – boxplot*

### 6.1.6 Turbidity

The turbidity values, measured in Nephelometric Turbidity Units between 01/04/2021 and 29/06/2021, are almost always close to zero. These values were gathered from the environmental probe. The sensor does not actually measure turbidity as such, but rather the refraction of light. A lot of refraction corresponds to a high turbidity.

The bacteria in the system are only active when they are residing in the biofilm. Outside the biofilm they are not active and there is no growth. At that time, turbidity is practically zero, which is why the curve is mainly flat. However, some peaks can be observed, which can be explained by the fact that the solution in the reactor has been changed, or by the fact that the bacteria are more active at certain times.

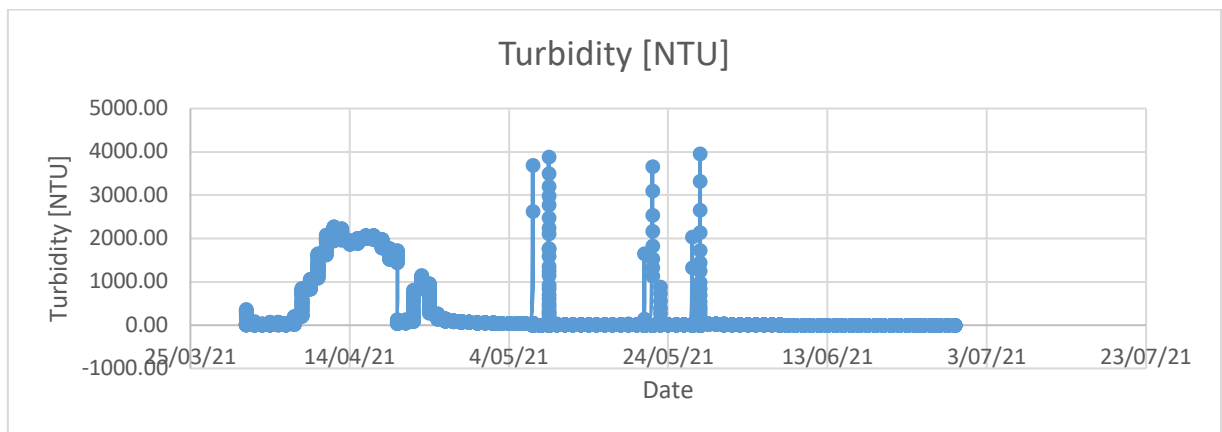


*Figure 30 Turbidity (NTU) measured between 01/04/2021 and 29/06/2021*

Representing the results as a boxplot (Figure 31), it appears that the majority of the values are around zero, with some rare exceptions reaching a maximum of 3876 NTU.

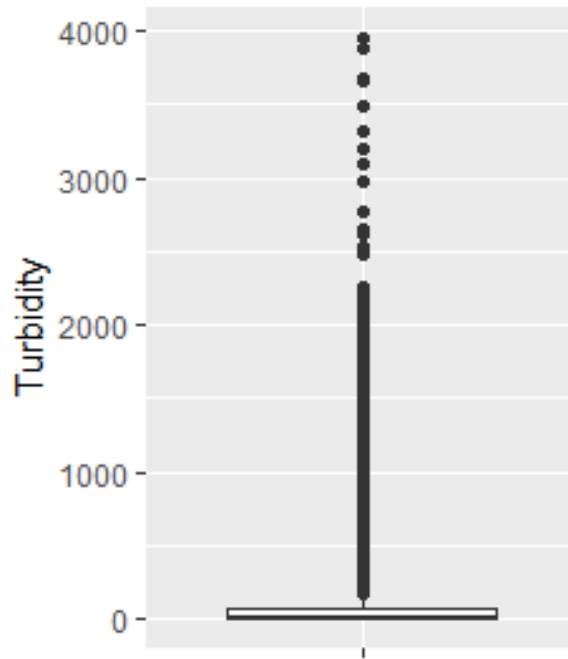


*Figure 31 Measured values of turbidity (NTU) – boxplot*

#### 6.1.7 Oxidation reduction potential

The oxidation reduction potential (ORP) of a liquid, also called redox potential, is a value that indicates how oxidizing or reducing the liquid is. An oxidizing environment is one in which a lot of oxygen is present. This oxygen gas tends to accept a lot of electrons, allowing oxidation reactions to take place. Since corrosion is an oxidation process, it is obvious that oxidising liquids are ideal for its formation. A reducing environment, on the other hand, is one in which there is no oxygen gas. Instead, these liquids usually contain other gases, called reducing agents, that tend to release electrons.

ORP can therefore be seen as the availability of electrons in an environment (relatively available in a reducing environment and relatively unavailable in an oxidizing environment). It is determined by measuring the potential of a chemically inert electrode immersed in the liquid to be studied. The potential of this electrode is read relative to a reference electrode, and the resulting value is expressed in millivolts. Reducing environments are represented by a negative value, while oxidizing liquids are represented by positive values (Nordstrom & Wilde, 2005; YSI Incorporated, 2021).

The values measured by the probe between 01/04/2021 and 29/06/2021 are mostly negative (Figure 32), meaning that the reactor is filled with a reducing liquid (which makes sense because the probe was placed in the anoxic reactor).

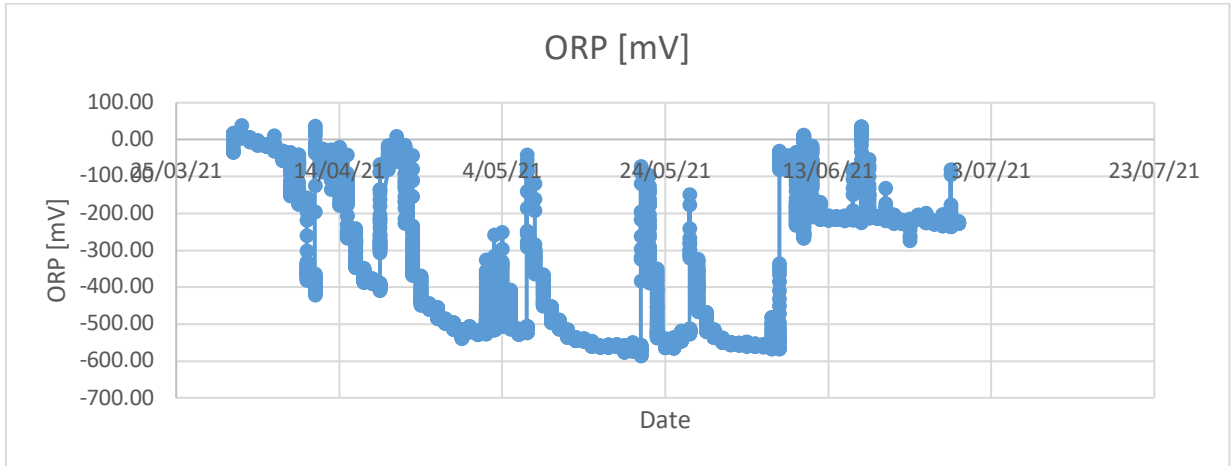


*Figure 32 Oxidation reduction potential (mV) measured between 01/04/2021 and 29/06/2021*

The quartile analysis of this variable (Figure 33) shows that most of the values obtained are between -205.30 and -522.80 mV. Although there are some maxima that can reach a value of 36.40 mV, it is clear that the majority of the values are negative, which proves once again that we are dealing with a reducing liquid (and an anoxic environment).

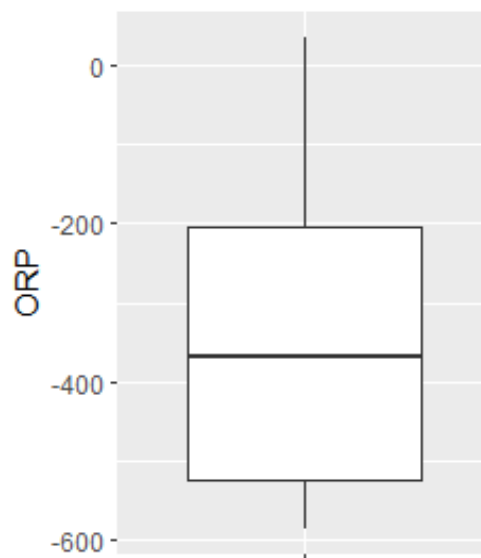


*Figure 33 Measured values of ORP (mV) – boxplot*

### 6.1.8 Corrosion rate

The corrosion rate values were obtained in two different ways. On the one hand, data were gathered after measurement by the LPR probe. On the other hand, a potentiodynamic measurement was performed. In order to determine which of these methods was the most accurate, a mass loss measurement was made.

#### 6.1.8.1 Measurement of the corrosion rate by the LPR probe

As explained in point 4.2, this probe measures the current produced by two electrodes after transmission of a certain voltage. The values obtained with the LPR probe are shown in Figure 34.

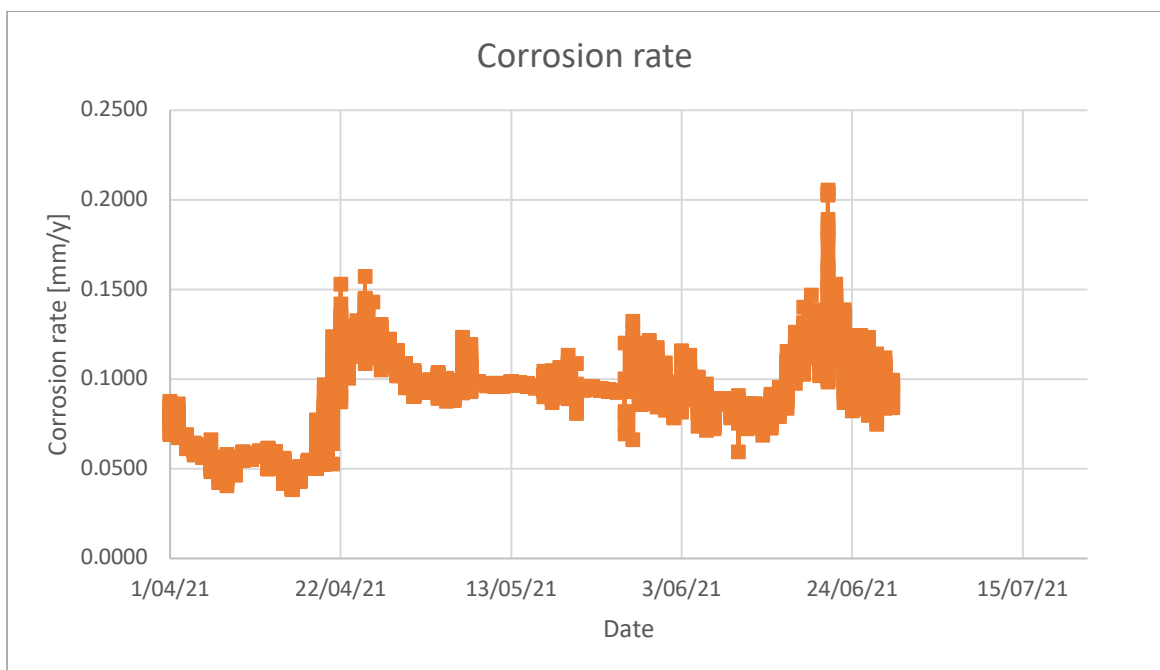


*Figure 34 Corrosion rate (mm/y) measured between 01/04/2021 and 13/07/2021*

As the graph of these data shows very large variations, filters were applied to remove outliers and to keep only a representative data set.

The first filter in question is a first derivative filter (Figure 35 a). The initial curve shows some abrupt changes which can be explained by the fact that the LPR probe needs stabilisation and therefore sometimes gathers values that are not relevant because they are only artefacts that do not correspond with real changes in the system. By calculating the first derivative of the curve, it is possible to limit the data to a certain level by eliminating noise from the graph (when variation from that level is too high, the values are removed).

The second filter used is called a Savitzky-Golay filter (Figure 35 b), that is also applied in order to increase precision. This filter is based on convolution, which is a process by which two functions are used to create a third function. This process uses a low-degree polynomial to fit successive subsets of adjacent data points. A convolution coefficient is then calculated and applied to the centre point of each subset in order to smooth the signal (Savitzky, 1989).

The third filter used is an Exponential Moving Average filter (Figure 35 c). The moving average technique is a technique whereby data is analysed by creating a series of averages of different subgroups of the initial database. A moving window is then taken (for a given point, an amount of data is averaged before and after that point by using an exponential function), and data varying outside of that window is left out. In this way, short-term fluctuations can be removed and only long-term trends, which are more relevant, are retained (Chou, 1975).

Each of these methods has pros and cons. The first derivative approach cuts out too much of the data and gives noise where there is actually no noise pattern, and it also ignores important parts of the curve (such as changes in corrosion rate created by different parameters). Although the other methods keep more data, they are not perfect either. The Exponential Moving Average method, for example, tends to overexplain the data. The Savitzky-Golay method, on the other hand, uses a lower degree polynomial than the Moving Average method, thus allowing not only to keep more data but also to take into account fluctuations caused but regular changes to the system (which is the case in this experiment since some of the environmental parameters were changed on a regular basis).

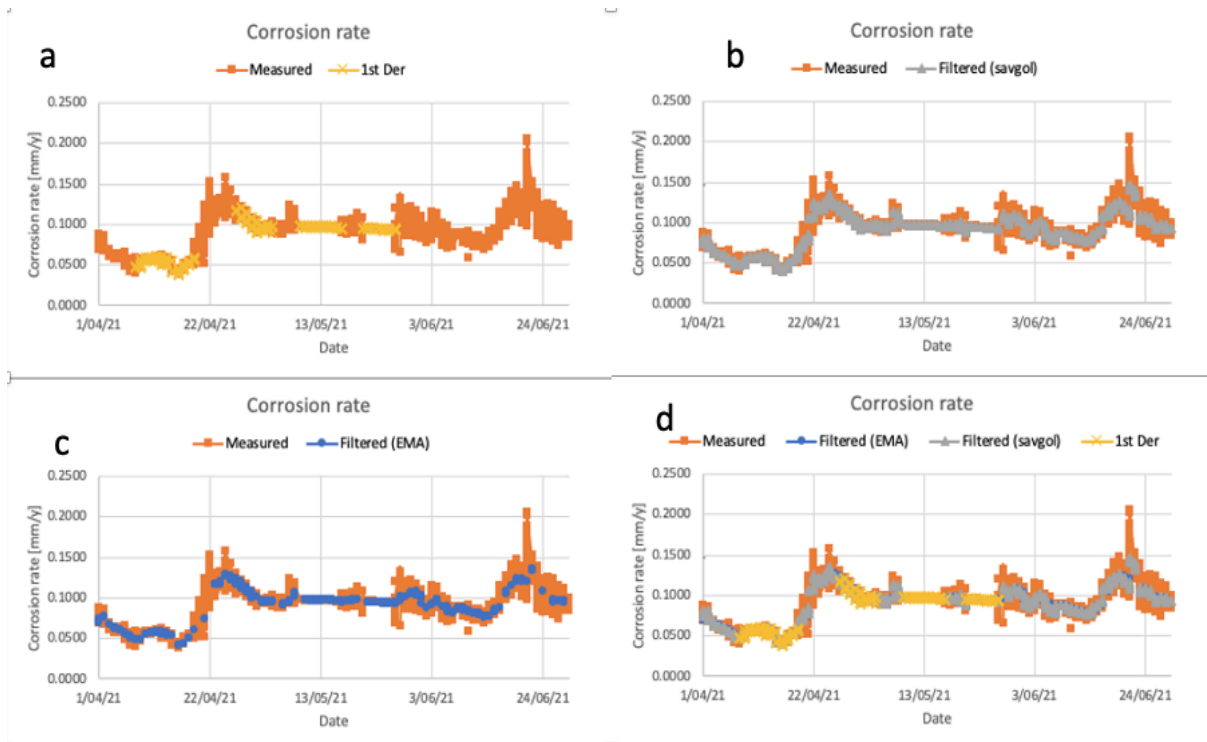


**Figure 35** Corrosion rate (mm/y) with filters - measurements from 01/04/2021 to 13/07/2021  
*a: measured date with 1<sup>st</sup> derivative filter; b: measured data with Savitzky-Golay filter; c: measured data with EMA filter; d: measured data with all filters combined*

Based on the curves obtained after applying each filter, boxplots (Figure 36) were made in order to compare the three methods and to determine the most relevant one for this experiment.

At first sight, it seems that the method with the most different values is the Exponential Moving Average method. Indeed, it shows a much smaller standard deviation than the other methods. However, this does not mean that the method is bad because it still allows a large amount of data to be kept in the dataset.

Another interesting observation is that it seems that the average corrosion rate calculated by the LPR probe does not change regardless of the filter applied. Indeed, if we focus on the values obtained for each dataset, it appears that the average value for corrosion rate without filter is 0.090548683 mm/year with a standard deviation of 0.022833021. After application of the Savitzky-Golay filter, the average corrosion rate is 0.089111546 mm/year with a standard deviation of 0.021500983. For the values obtained with the first derivative approach, the average rate is 0.082194374 mm/year with a standard deviation of 0.021549104. The EMA filter, on the other hand, gives a data set with a mean value of 0.092754326 mm/year and a standard deviation of 0.015533352 which is indeed smaller than the standard deviations of the other datasets.

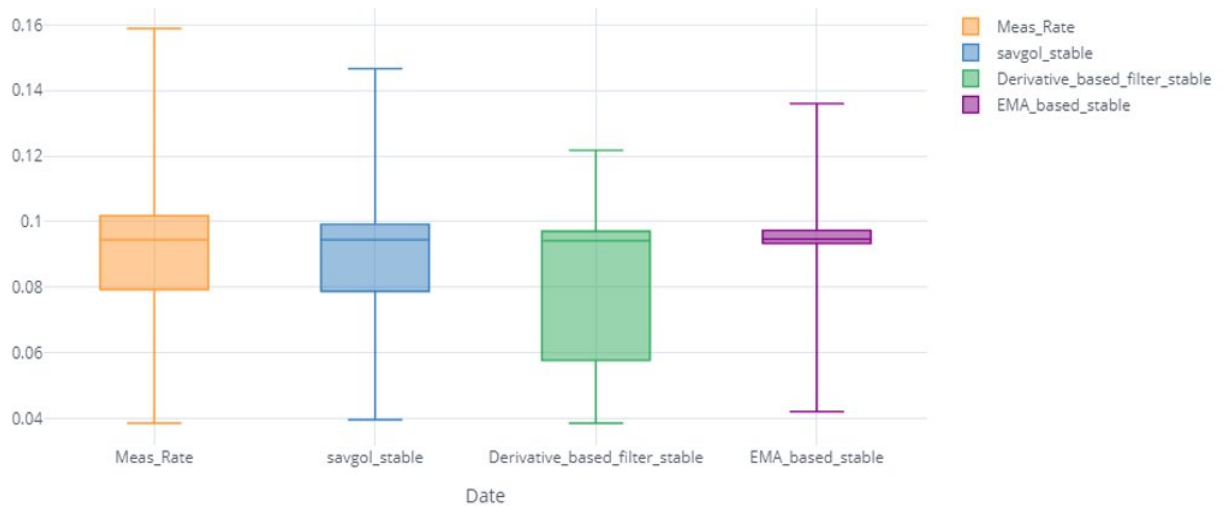


**Figure 36** Statistical analysis of the filtered data

#### 6.1.8.2 Potentiodynamic measurement

With this method, the potential (E) was measured relative to the current density. The slope of the curve was measured, and the result obtained for this slope is called polarization resistance value, which can be used to calculate a corrosion rate. This potentiodynamic measurement was carried out in four tests. The first test did not give reliable results because it was carried out immediately after the metal coupons were immersed in the reactor, at which time the coupons were still very clean (which means passivation takes place very quickly). The other three tests are considered to be more reliable as they show a good alignment with each other (the curves on Figure 37 approach each other since the potential stabilizes).

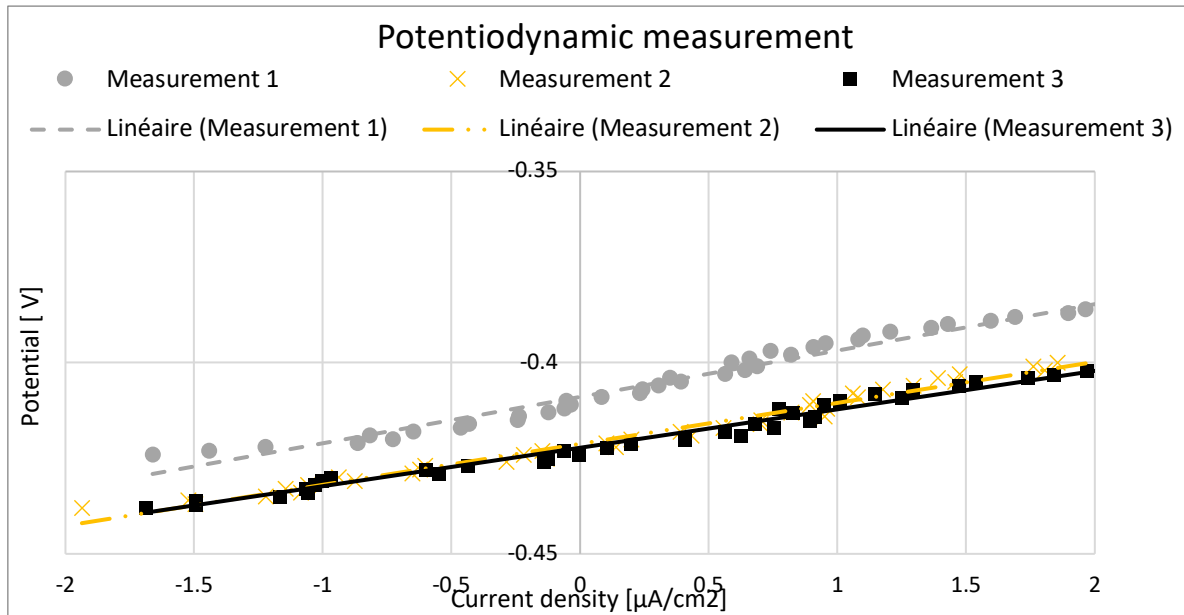


*Figure 37 Potentiodynamic measurement*

### 6.1.8.3 Mass loss measurement

The average value obtained for the corrosion rate after performing the last three potentiodynamic tests is 0.01855 mm/year, which is about 10 times higher than the results obtained by the LPR probe. It would seem sensible to rely on the potentiodynamic test, but the two measurement methods showing such a discrepancy, a third technique should be used as a check. For this reason, a mass loss measurement was carried out.

On 29/07/2021, the metal coupons were removed from the reactor and cleaned (Figure 38 shows coupons before and after cleaning).

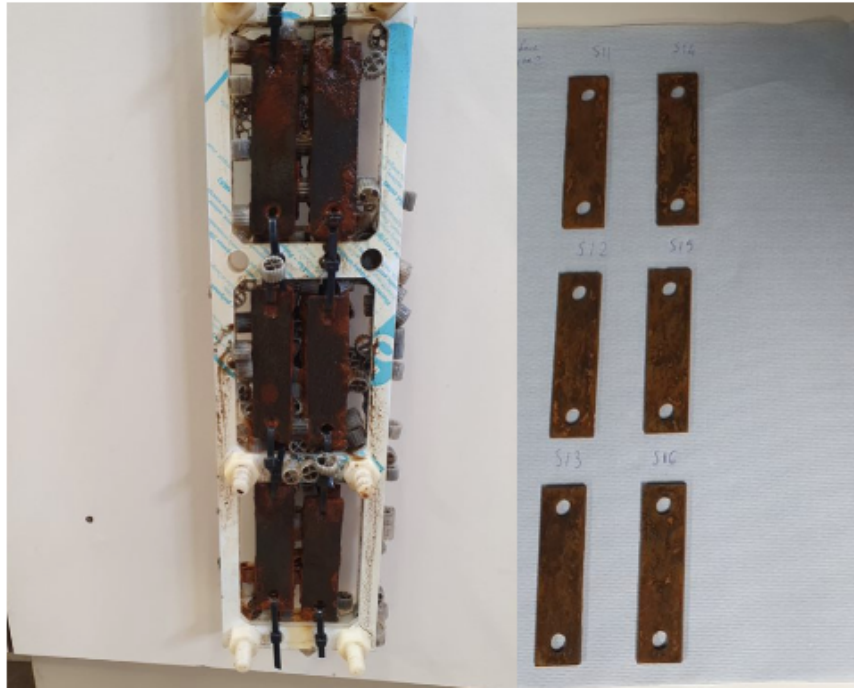


*Figure 38 Mass loss measurements - coupons before and after cleaning*

The coupons were cleaned in six cycles and weighed after each cycle. All measured weights can be found in Table 9. As three coupons were damaged during manipulation, their weight was not measured nor will the coupons be used for further experiments.

*Table 9 Weight of coupons after each cleaning cycle*

<b>CYCLE 1</b>	<b>S1L</b>		<b>S1R</b>	
	<b>1</b>	34.4803 g	<b>4</b>	34.2115 g
	<b>2</b>	34.5387 g	<b>5</b>	34.5401 g
	<b>3</b>	34.8876 g	<b>6</b>	34.775 g
	<b>S2L</b>		<b>S2R</b>	
	<b>1</b>	34.2328 g	<b>4</b>	NA
	<b>2</b>	34.6264 g	<b>5</b>	NA
	<b>3</b>	34.2684 g	<b>6</b>	NA
<b>CYCLE 2</b>	<b>S1L</b>		<b>S1R</b>	
	<b>1</b>	34.4748 g	<b>4</b>	34.2057 g
	<b>2</b>	34.5316 g	<b>5</b>	34.5381 g
	<b>3</b>	34.5316 g	<b>6</b>	34.7729 g
	<b>S2L</b>		<b>S2R</b>	
	<b>1</b>	34.227 g	<b>4</b>	NA
	<b>2</b>	34.6188 g	<b>5</b>	NA
	<b>3</b>	34.2622 g	<b>6</b>	NA
<b>CYCLE 3</b>	<b>S1L</b>		<b>S1R</b>	
	<b>1</b>	34.4729 g	<b>4</b>	34.2037 g
	<b>2</b>	34.5308 g	<b>5</b>	34.538 g

	<b>3</b>	34.8771 g	<b>6</b>	34.773 g
	<b>S2L</b>		<b>S2R</b>	
	<b>1</b>	34.2257 g	<b>4</b>	NA
	<b>2</b>	34.6184 g	<b>5</b>	NA
	<b>3</b>	34.2618 g	<b>6</b>	NA
<b>CYCLE 4</b>	<b>S1L</b>		<b>S1R</b>	
	<b>1</b>	34.4707 g	<b>4</b>	34.2028 g
	<b>2</b>	34.5319 g	<b>5</b>	34.5387 g
	<b>3</b>	34.8771 g	<b>6</b>	34.7733 g
	<b>S2L</b>		<b>S2R</b>	
	<b>1</b>	34.2265 g	<b>4</b>	NA
	<b>2</b>	34.6188 g	<b>5</b>	NA
	<b>3</b>	34.2618 g	<b>6</b>	NA
<b>CYCLE 5</b>	<b>S1L</b>		<b>S1R</b>	
	<b>1</b>	34.47 g	<b>4</b>	34.2022 g
	<b>2</b>	34.5318 g	<b>5</b>	34.5388 g
	<b>3</b>	34.8769 g	<b>6</b>	34.7735 g
	<b>S2L</b>		<b>S2R</b>	
	<b>1</b>	34.2264 g	<b>4</b>	NA
	<b>2</b>	34.6188 g	<b>5</b>	NA
	<b>3</b>	34.2618 g	<b>6</b>	NA
<b>CYCLE 6</b>	<b>S1L</b>		<b>S1R</b>	
	<b>1</b>	34.4699 g	<b>4</b>	34.2019 g
	<b>2</b>	34.5315 g	<b>5</b>	34.5391 g
	<b>3</b>	34.8769 g	<b>6</b>	34.7741 g
	<b>S2L</b>		<b>S2R</b>	
	<b>1</b>	34.2267 g	<b>4</b>	NA
	<b>2</b>	34.6185 g	<b>5</b>	NA
	<b>3</b>	34.2628 g	<b>6</b>	NA

After each cycle, the weight of the coupons was compared with the initial weight (weight before the first immersion as indicated in Table 8) in order to determine the weight loss between the date of the first immersion in the reactor and the date of the test (the weight loss calculated after each cleaning cycle is represented in Figure 39).

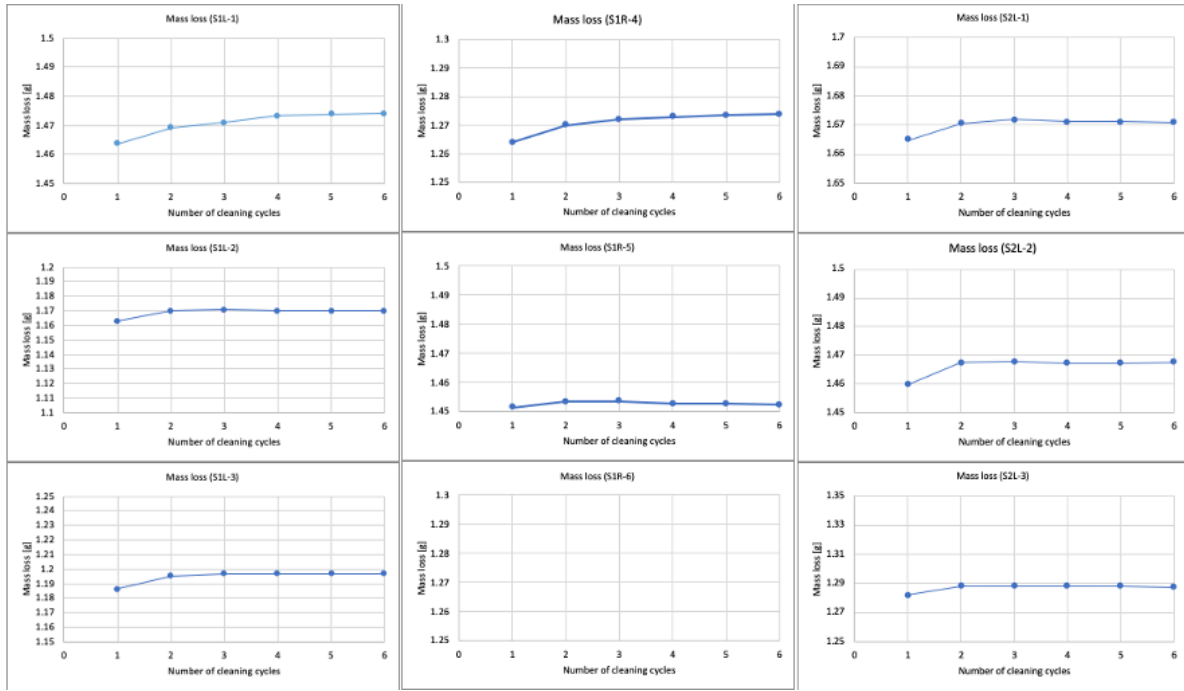


**Figure 39** Mass loss of coupons after each cleaning cycle

By using these values in Equation 10 (ASTM International & G01 Committee, n.d.), the rate at which corrosion occurred for each coupon during this specific time period could be determined.

$$\text{Corrosion rate} = (K*W) / (A*T*D) \quad (\text{Eq. 10})$$

where K is a constant of 87600; W represents the mass loss in grams; A is the area of the coupons in cm<sup>2</sup> (108,072 cm<sup>2</sup>); T is the time of exposure in hours (3091,50 hours); D is the density in g/cm<sup>3</sup>.

The mean value obtained after calculation of all individual corrosion rates is 0,045320138 mm/year, which is of the same order of magnitude as the value obtained with the potentiodynamic measurement (Figure 40). This confirms the fact that the data obtained during those four tests are probably more reliable than those gathered with the LPR probe.

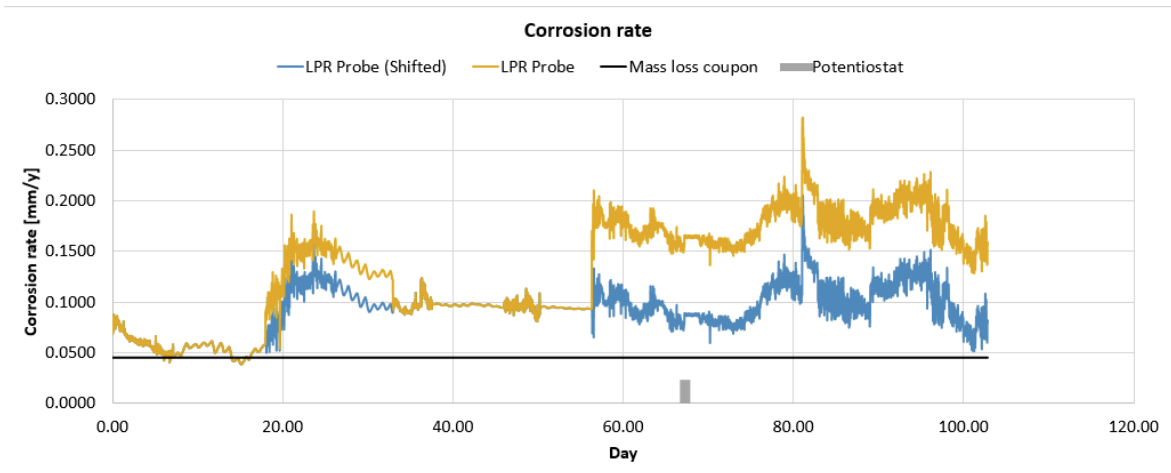


*Figure 40 Comparison of LPR probe method, potentiodynamic test and mass loss measurement*

*(Due to an electricity breakdown at the site of the experiment, data gathered by the LPR probe were inaccurate and had to be shifted in order to correspond with the real values in the reactor)*

An explanation as to why the LPR probe is less reliable than the two other methods is that it is directly affected by the process (because it is in contact with the environment in the reactor). For the purpose of the experiment, the process is constantly being changed. Because we are looking at something, we change the process, but because the process changes it also changes the way we are looking at it.

## 6.2 Correlation analysis

### 6.2.1 One-on-one correlation between parameters

As explained in section 5.1, several of the environmental parameters may be interdependent. It is therefore relevant to study the relationship between these different parameters to try to understand how they influenced each other in the anoxic reactor. To this end, the correlation between all of these factors was graphically represented as a series of scatterplots. Figure 41 shows each of these scatterplots. On the horizontal axis, the different parameters are correlated one by one. The distribution of each parameter is shown on the diagonal of the image and thus separates the scatterplots from the different Pearson coefficients ( $r$ ) which numerically represent the correlation between two sets of data (Benesty, Chen, Huang, & Cohen, 2009). This coefficient is obtained by calculating the ratio between the covariance of the two variables and the product of their standard deviations. It ranges from -1 (negative correlation) to 1 (strong positive correlation).

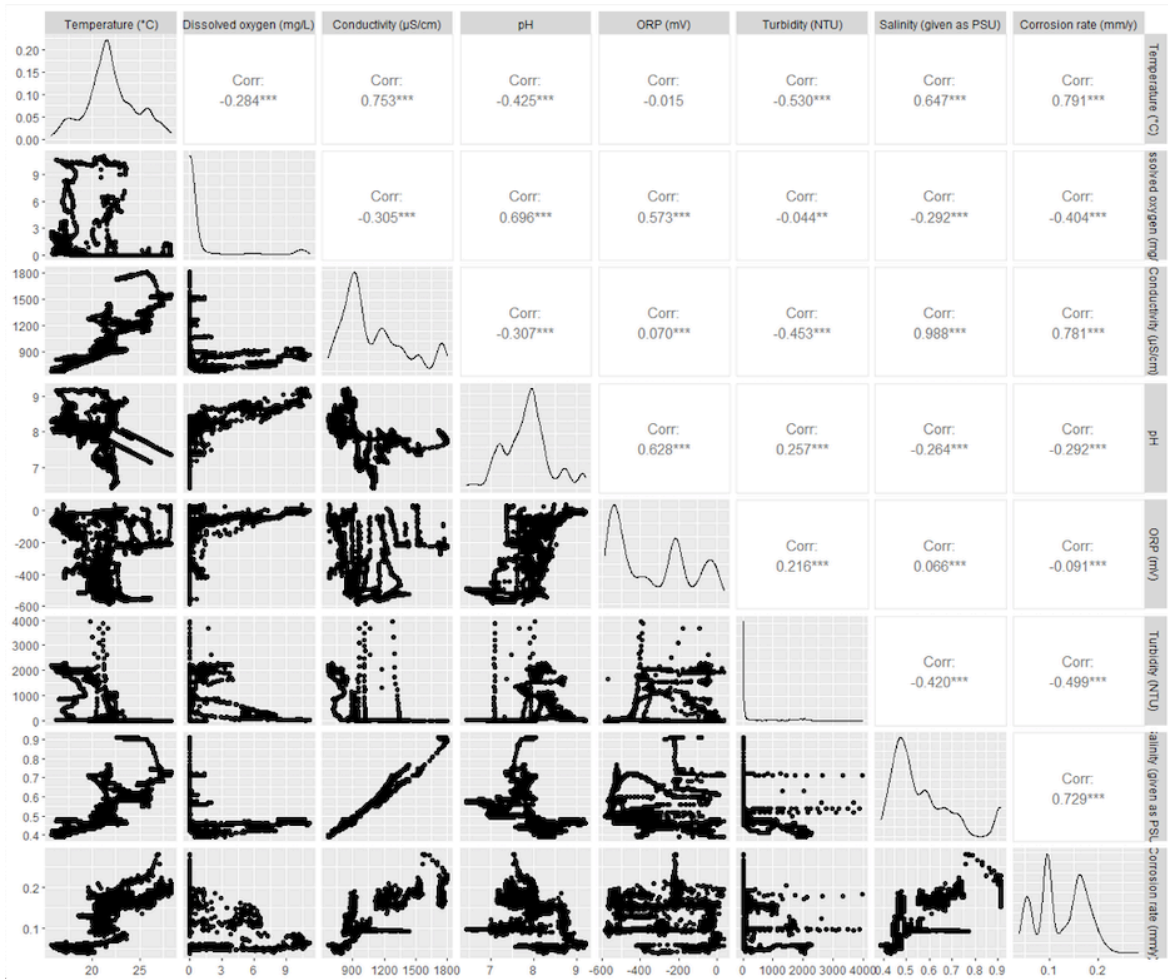


Figure 41 Correlation between the parameters measured by the environmental probe

### 6.2.1.1 Temperature

As can be seen from Figure 34, temperature does not show any positive correlation with dissolved oxygen, ORP and turbidity. However, there is clearly a correlation between the temperature of the liquid and its conductivity (with a  $r$  of 0.753) as well as its salinity (with a  $r$  of 0.647). These two parameters increase with increasing temperature.

Another relationship that can be observed is the one between the temperature and the pH of the liquid (the graph indicates a decreasing pH for an increasing temperature and the value of the Pearson correlation coefficient is -0.425). The pH is a way of quantifying the concentration of  $H^+$  ions present in a solution. According to Le Chatelier's principle, by changing the conditions of a reaction in equilibrium, the equilibrium position will move to counteract this change. Thus, by increasing the temperature of a solution, the equilibrium will shift to decrease the temperature again by absorbing the additional heat. This is associated with an increase in molecular vibrations, thus forming more hydrogen and

hydroxide ions (as the medium will be less likely to form hydrogen bonds). The result is a drop in pH, as observed (Clark, 2013; Pawlowicz, 2013; Reagecon, n.d).

Finally, the scatter plot also shows that the corrosion rate increases with increasing temperature ( $r$  being 0.791).

#### 6.2.1.2 *Dissolved oxygen*

The dissolved oxygen concentration in the reactor increases with pH and ORP (the correlation between dissolved oxygen and ORP has already been explained in section 6.1.7).

However, there seems to be a negative correlation ( $r$  of -0/404) between dissolved oxygen and corrosion rate (increasing corrosion rates with lower dissolved oxygen concentration). These results are rather unreasonable and could be explained by the fact that the turbidity and dissolved oxygen concentration were very low in the reactor (the former due to bacteria being active on the carriers and not in the solution, the latter due to the anoxic conditions in the reactor).

#### 6.2.1.3 *Conductivity*

There is a very strong correlation ( $r$  of 0.988) between conductivity and salinity. This is because conductivity is the ability of a liquid (in this case the water in the reactor) to pass an electrical flow. This capacity depends on the concentration of ions present in the liquid. These ions come from compounds that dissolve in water (also called electrolytes), of which salts are a part. Indeed, salts dissolve in water and form anions (negatively charged particles) and cations (positively charged particles) which are the basis of conductivity. The more ions (anions and cations) there are in the liquid, the more conductive it is. Therefore, since salinity is the total concentration of dissolved salts in the liquid, the higher the salt concentration, the more ions, the more conductive the liquid.

A correlation between conductivity and temperature can also be observed ( $r$  of 0.753). Indeed, increasing the temperature of a liquid can lead to an increase in ionic mobility as well as a greater solubility of the salts present in the liquid. This implies a higher conductivity (Barron & Ashton, 2007; Chang et al., 2011; Cole-Parmer, 2021; Fondriest Environmental, Inc., 2014).

There is therefore obviously a positive correlation ( $r$  of 0.781) between conductivity and corrosion rate.

#### 6.2.1.4 Turbidity

The scatter plot (Figure 41) shows a negative correlation between the turbidity and the temperature of the liquid ( $r$  value of -0.530).

Another correlation that can be observed is an increasing corrosion rate with lower turbidity (the  $r$  value of -0.499 indicates a negative correlation between those two parameters), which is a rather illogical result. It should be expected that turbidity increases the likelihood of corrosion. The reason for these results remains to be determined.

#### 6.2.2 Correlation of each parameter with corrosion

As mentioned in 6.2.1, several parameters show a correlation with corrosion. In order to better understand this correlation, a Principal Components Analysis (PCA) was performed (Hartmann, Krois, & Waske, 2018). With this PCA, different variances were calculated, giving several principal components (PC) which correspond to variables that are decorrelated from each other (this is a way of transforming related variables into new variables in order to make the information less redundant). A total of seven principal components was obtained, but the variation of the last one being zero, only six were considered (Figure 42).

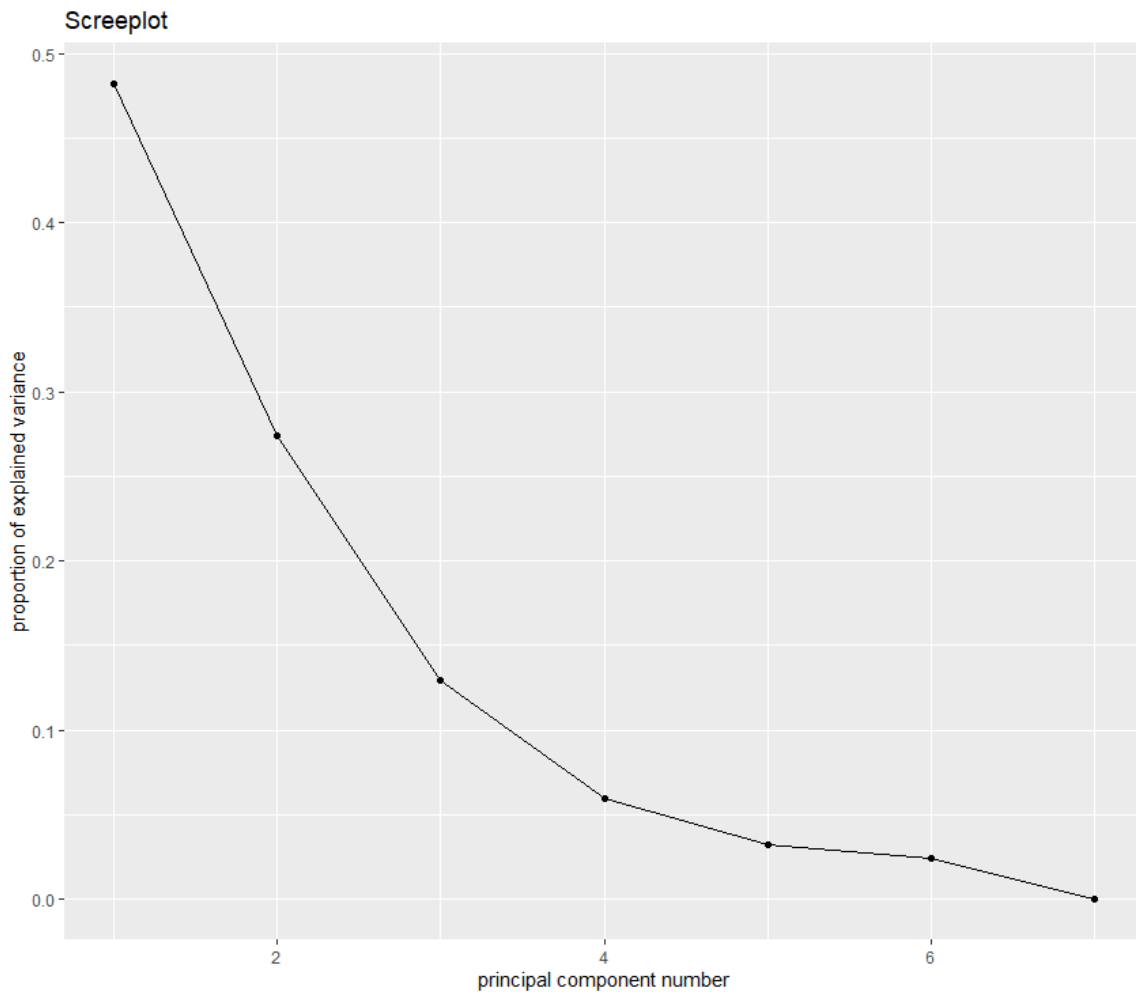


**Figure 42** *Screenplot - total number of principal components obtained from PCA*

As only the principal components representing more than 10% of the explained variance are relevant for a statistical analysis, three of those six components (PC1 which represents an explained variance of 51%, PC2 with an explained variance of 24.4% and PC3 with an explained variance of 11.3%) were used to create biplots, which are plots showing both variables and observations in the same space.

The biplots are representations of the contributions of each individual parameter and are therefore divided into axes called principal components axes which explain an acceptable level of variance (Kaiser, 1961; Peres-Neto, Jackson, & Somers, 2005; Young, 1999).

The correlation circle represents the correlation between a variable and a principal component.

Positively correlated variables are grouped together on the plot. Negatively correlated variables are positioned on opposite sides (opposite quadrants) of the origin of the graph.

The distance between the variables and the origin measures the quality of the representation of the variables (variables that are far from the origin are well represented for the chosen explained variance, meaning that the closer a variable is to the correlation center, the more important it is for interpreting the components under consideration (Abdi & Williams, 2010; Husson, Lê, & Pagès, 2017)).

In the first graph, the horizontal axis corresponds to PC1 and the vertical axis to PC2 (Figure 43). For these values, it is possible to see a strong correlation between corrosion rate and temperature since their two vectors are almost identical in length and orientation, and the angle between them is very small. Salinity and conductivity are also represented in the same quadrant as corrosion rate, showing a positive correlation between the variables. However, ORP, dissolved oxygen and pH are represented in a different quadrant at an almost right angle, indicating that these variables do not show a similar response profile to corrosion rate. The turbidity vector, on the other hand, is in the direct opposite direction to the corrosion vector. The two variables are therefore negatively correlated, as explained in 6.2.1.4.

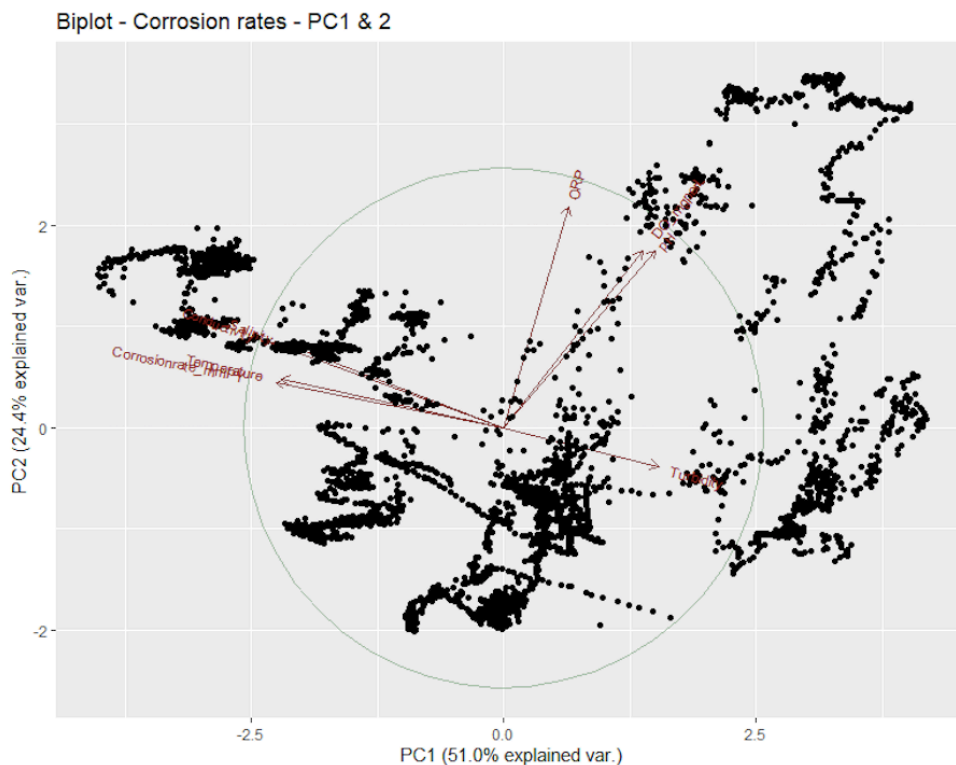


*Figure 43 Corrosion rates biplot - PC1 & PC2*

The second graph relates PC1 to PC3 (Figure 44). In this plot, the length of some vectors (dissolved oxygen, pH and ORP) is much shorter, indicating that these variables are not well

represented for the chosen explained variances. Again, the vectors for temperature, salinity and conductivity are plotted in the same quadrant as that for corrosion rate, indicating a positive correlation between the variables. The direction of the pH vector is almost directly opposite to that of the corrosion vector, indicating that there would be a strong negative correlation between the two variables. However, this is not consistent with the results obtained from the other statistical studies (discussed in paragraph 6) and is explained by the fact that the pH variable is not well represented on this plot. Indeed, although there is a negative correlation between the two variables, this correlation is quite weak ( $r$  of -0.292 on Figure 41), which is not the case on this graph.

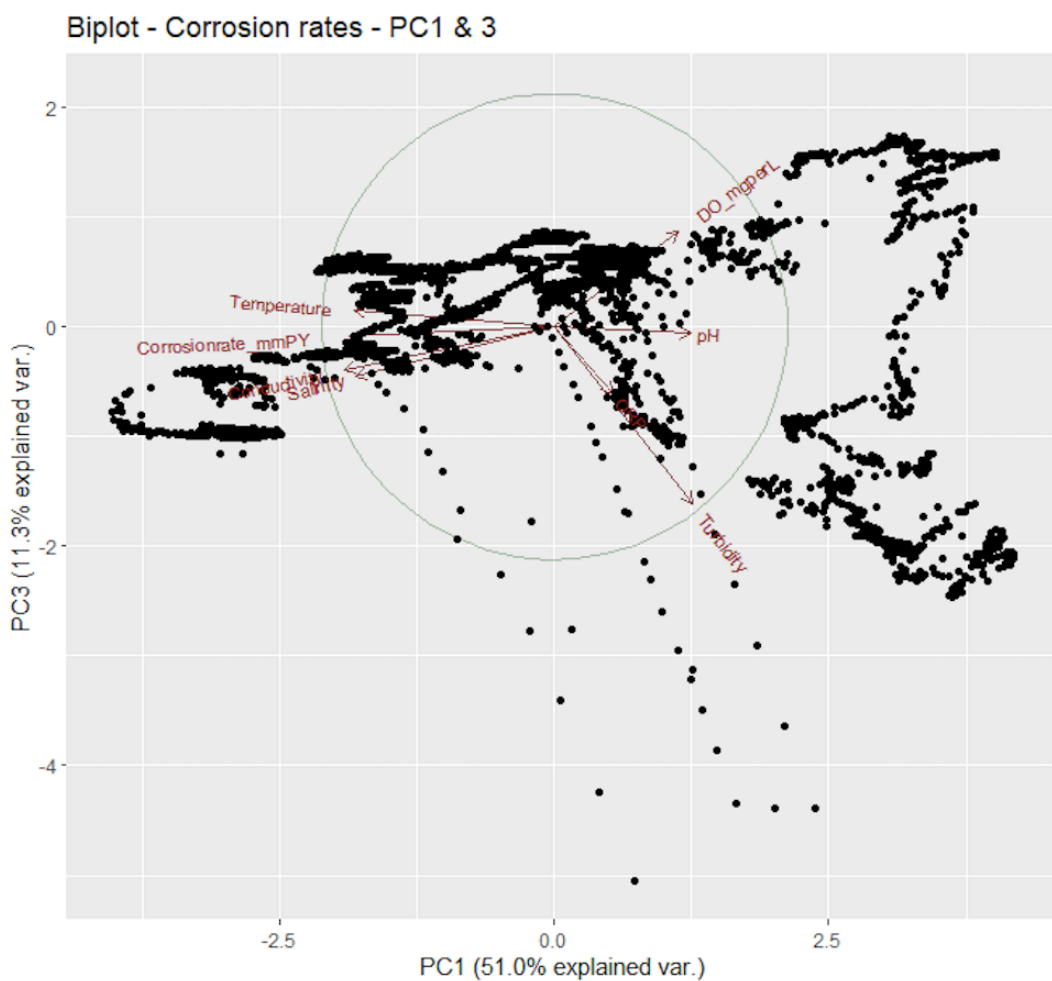


*Figure 44 Corrosion rates biplot - PC1 & PC3*

The third biplot shows PC2 on the horizontal axis and PC3 on the vertical axis (Figure 45). In this graph, the vectors for pH, conductivity, salinity and temperature are far from the correlation circle, indicating that these variables are poorly represented and do not allow for a correct interpretation of the components under consideration. ORP, on the other hand,

shows a very strong correlation with corrosion rate, which was not the case in the previous statistical analysis (Figure 41). On this view, the vectors representing corrosion rate and turbidity are almost orthogonally positioned, which shows a lack of correlation between the two variables. The latter interpretation is also at odds with previous observations.

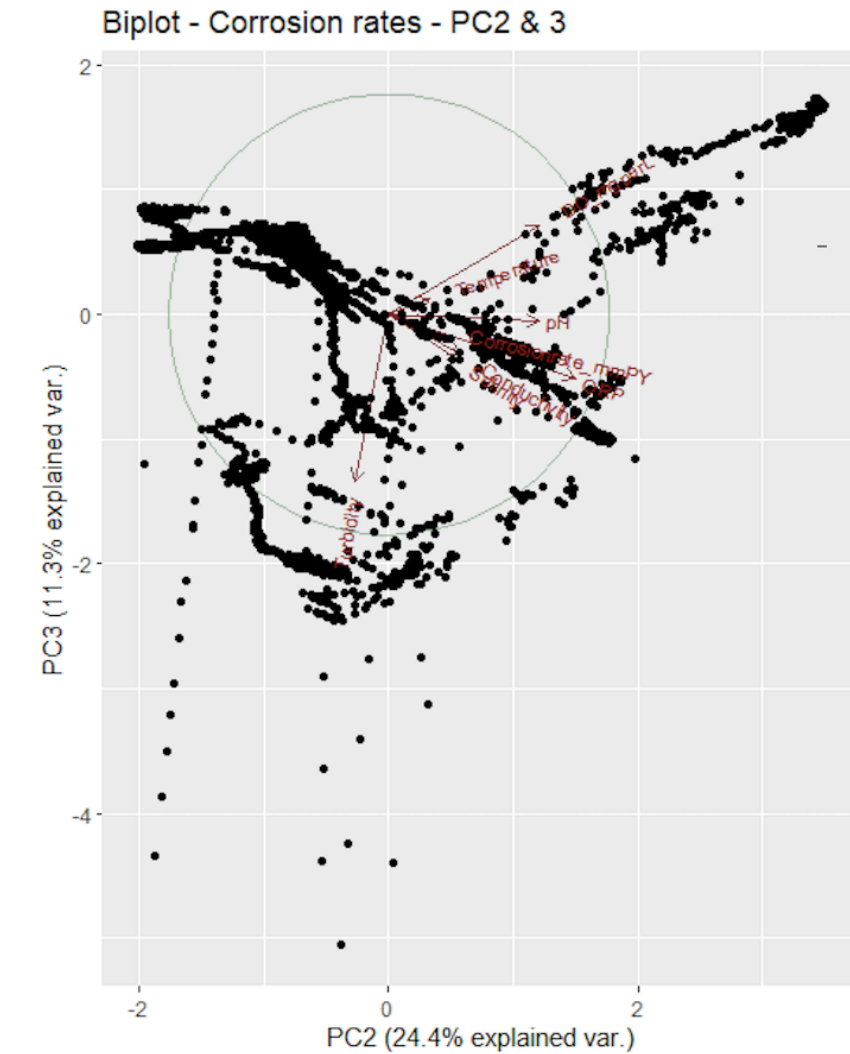


Figure 45 Corrosion rates biplot - PC2 & PC3

### 6.3 Functional analysis

#### 6.3.1 Pourbaix diagram

A Pourbaix diagram is a diagram based on the Nernst equation (Equation 11), which is an equation relating the equilibrium potential of an electrode to its standard potential and to the concentrations or pressures of chemical species undergoing reduction or oxidation at a

certain temperature (as a general rule, the Pourbaix diagram is plotted at a temperature of 25°C).

$$E = (E^{\circ} - (RT/nF)) * \ln([reduced] / [oxidized]) \quad (\text{Eq. 11})$$

where E is the equilibrium potential of the electrode (in mV); E° is the standard potential of the electrode; R is the universal gas constant (8.314462 J/molK); T is the absolute temperature (in °C); n is the number of moles of electrons involved in the reaction; F is the Faraday constant (96485 C/mol); [reduced] represents the product of the concentrations of all species appearing on the reduced side of the reaction raised to the power of their stoichiometric coefficient; [oxidized] represents the same for the oxidized side of the reaction (Thompson & Kateley, 1999).

This equilibrium potential (E) between the metal and its various oxidised species is plotted on the Pourbaix diagram as a function of the pH. This potential is usually given in relation to the normal hydrogen electrode. The diagram thus shows the different domains of existence of the various states of an element (these different states being passivity, immunity and corrosion). In other words, it allows us to determine which species (metals or alloys) are thermodynamically stable at a certain potential and pH.

Since the potential is represented on the y-axis, the top of the diagram represents the most oxidized regions of an element. As the pH is represented on the x-axis, the areas on the left are the most acidic forms and those on the right the most basic forms of that element.

On the diagram, several lines can be observed.

The horizontal lines represent electron transfer reactions. These are dependent on potential but not on pH. The vertical lines, on the other hand, are dependent on pH and not on potential and are not accompanied by electron transfer. The slanting lines, on the other hand, give the redox potentials of a solution in equilibrium, indicating both electron transfer and a certain pH (Pourbaix, De Zoubov, & Van Muylder, 1963).

The purpose of the diagram is to show the direction of different reactions at a certain pH and potential. It serves as a basis for estimating corrosion since it shows which environmental changes will increase or decrease it.

However, it has some limitations, namely that it only shows reactions between pure metals, pure water and the species that can be formed from them. Furthermore, it is constructed from thermodynamic data and therefore does not provide any data on the velocity of the reactions (no kinetic data). Since they are constructed at a temperature of 25°C, they also do not provide information on temperature changes, which are essential in determining the corrosion rate.

Based on the data collected from the experiment in the anoxic reactor, a Pourbaix diagram was drawn (Figure 46).

The y-axis shows the redox potential, ranging from -1200 mV to 1600 mV. On the x-axis, the pH is represented for values ranging from -2 to 16.

On this diagram, the equilibrium state of the different species of the element iron (Fe) can be observed. Indeed, as the metal coupons studied are alloys of iron, it is this element that is represented. The species studied (the one composing the coupons used in the experiment) is predominant between the blue lines on the graph. Above and below these lines, the molecule is no longer stable. It is therefore between these two lines, and thus between these values of redox potential and pH, that corrosion takes place.

If we replace the values obtained for the corrosion rate on this diagram, we can see that the corrosion rate is highest for a pH varying between 6 and 9 and a redox potential ranging from -400 mV to approximately 300 mV. These pH values are logical since the reactor is kept at a more or less neutral pH. It would therefore have been impossible to obtain results at other values.

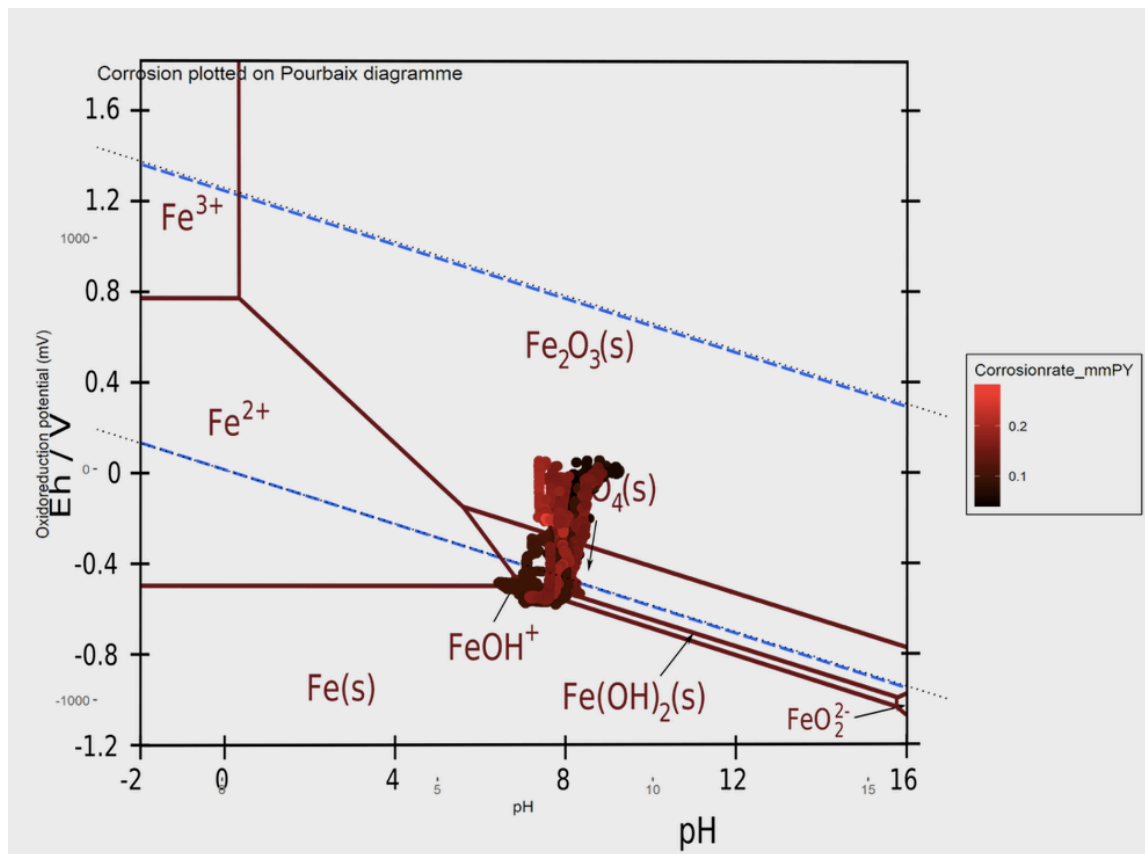


Figure 46 Corrosion rate plotted on a Pourbaix diagram

### 6.3.2 Evans diagram

The LPR probe measures the corrosion potential, i.e. the open circuit potential at the moment when the electrode is stabilised in the environment to be studied (the system has an equilibrium relationship between the three electrodes, which is characterised by a fall in potential followed by stable values).

Furthermore, by performing a polarisation test (either a static polarisation test or a potentiodynamic test), it is possible to calculate the corrosion current.

These two values (current and potential) can then be used to make a Tafel plot, which is a plot showing the relationship between the current in an electrochemical cell and the electrode potential of a metal and is generally used for studying and predicting corrosion rates.

In a Tafel plot, the potential does not correspond to a fixed current, but to a zero current (which is why the beginning of the graph is stable). In other words, the open circuit potential is obtained when there is no current flow.

In the anoxic bioreactor, a series of four measurements was carried out on a specimen. For this purpose, three electrodes (working electrode, i.e. the metal coupon; reference electrode and counter electrode, i.e. the electrodes present on the LPR probe) were placed in the system. After waiting 15 minutes, stabilisation was reached. The potentiostat was then instructed to apply a certain potential to the system while specifying a margin around this value (in this experiment a margin of 20 mV was chosen, which is a very small margin that does not have a major influence on the metal coupon, which is why the test is a non-destructive test). The metal coupon, which then corrodes in an accelerated way because of the applied potential, gives a resistance to this potential. This resistance is the polarisation resistance and can be obtained by calculating the slope of the curve obtained after the test has been performed Figure 47. Although the four measurements taken gave different results, the slope of each of the four curves is exactly the same, meaning that the resistance is also the same.

Since the polarisation resistance and the corrosion potential are known, it is possible to obtain the corrosion current by simply applying Ohm's law.

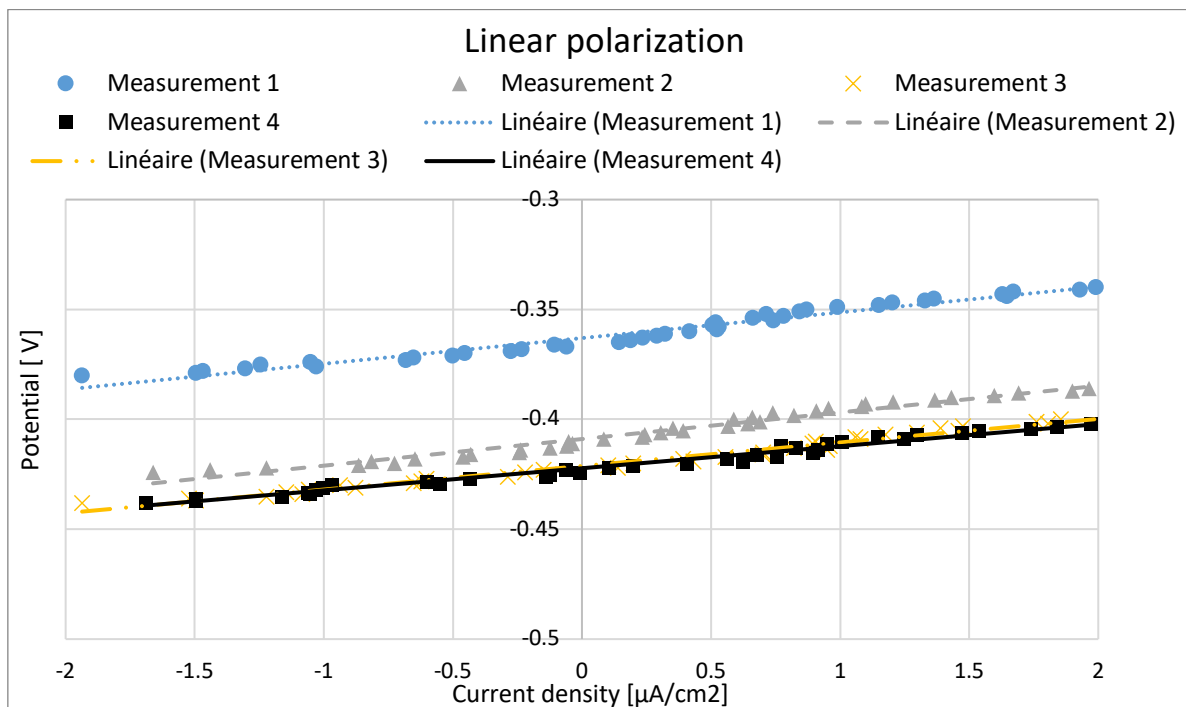


*Figure 47 Linear polarization curve*

The potential and current values obtained after the test were then taken as a Tafel plot (Figure 48).

However, as the polarisation curve is mainly influenced by one of the two reactions (either reduction for very cathodic potentials or oxidation for very anodic potentials), only the linear parts of the curve can be used to interpolate the Tafel plot values. A reliable interpolation would require observations over a few decades.

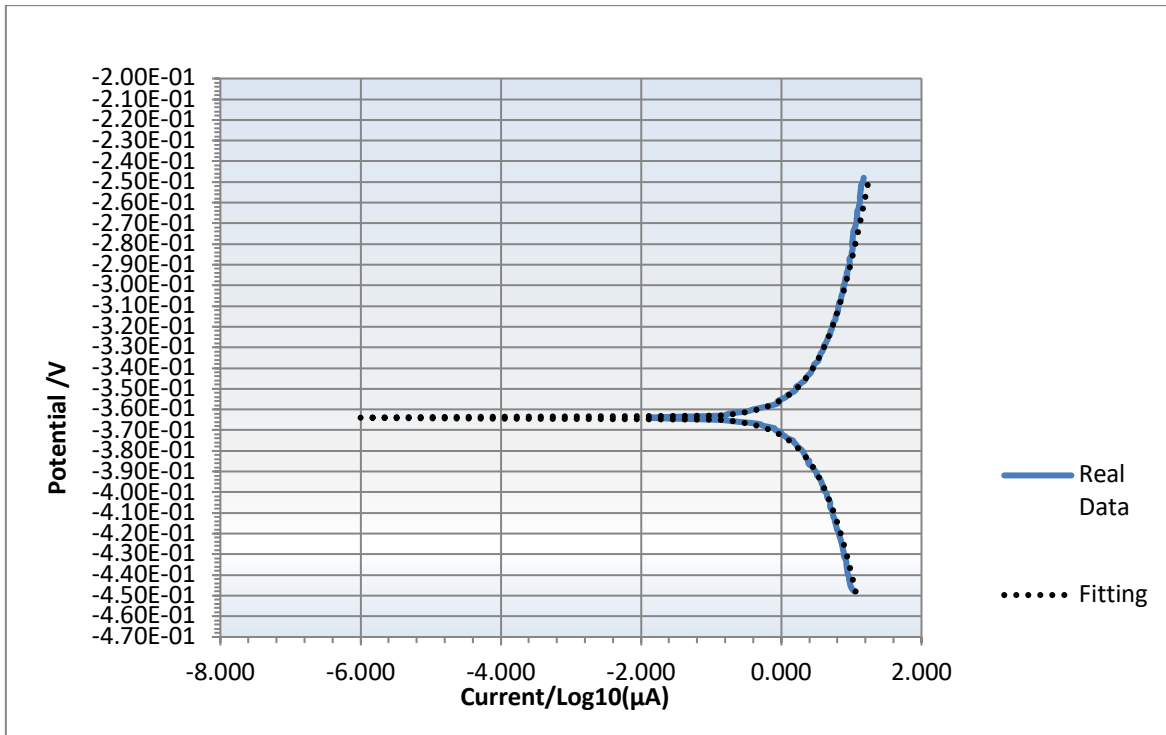


*Figure 48 Tafel plot for predicting corrosion rate*

By combining two Tafel plots (one for both side reactions) into one plot, an Evans diagram can be drawn (PalmSens, 2021). It represents the relationship between the current (usually represented in logarithmic form on the x-axis) and the oxidoreduction potential (on the y-axis). In other words, it is a representation of the electrode's kinetic data and its thermodynamics for both the oxidation and the reduction reaction (PalmSens, 2021).

Corrosion only happens when the total rate of oxidation is equal to the total rate of reduction (i.e., when all electrons released by the oxidation are accepted by the reduction). This is represented by the curves of the two reactions intersecting on the diagram (which means that if the intersection is known, the corrosion potential and the corrosion current are also known).

Figure 49 shows a general representation of an Evans diagram (this representation is for information purposes and is not based on the data from the experiment).

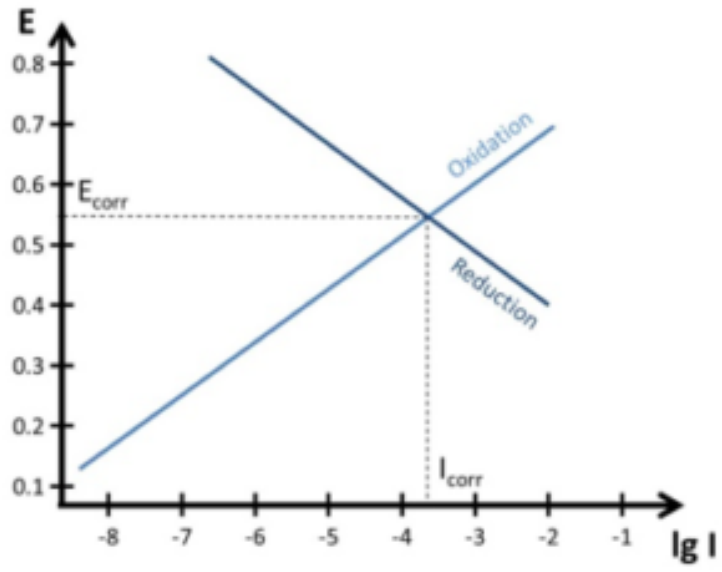


*Figure 49 General aspect of an Evans diagram*

(PalmSens, 2021)

## Conclusion

Corrosion, and more particularly aqueous corrosion, is a complicated electrochemical process in which several factors must be taken into consideration. In addition to the metallic composition of the corroded element, the environment in which the reaction takes place plays an important role. Indeed, several parameters of this environment influence the corrosion process. The study and understanding of this influence are complicated because of the interdependence between the different factors involved. Thus, depending on changes in one of the factors, the whole environment can be affected and the corrosion reaction on a metal part can be altered. Depending on the changes made and which factors have a greater impact than others, several types of corrosion can be observed.

In order to better understand the influence of these factors, Grade A steel coupons were placed in an anoxic bioreactor in which a water denitrification process takes place. Probes were placed in that same reactor to measure parameters such as pH, dissolved oxygen, temperature, redox potential, conductivity, turbidity, salinity and corrosion rate. It is expected that such a metal type under such conditions would corrode in a rather general way but also show signs of pitting or crevice corrosion, a hypothesis which was confirmed when taking the coupons out of the reactors after three months of immersion.

Before analysing the correlations between these factors, they were studied individually in order to have a clearer idea of the behaviour of each one. For example, it was observed that the temperature changed over time. This was explained by the fact that the reactor was kept at room temperature, which varied with the change of season, leading to higher temperatures at the end of the experiment than when the measurements were first taken three months earlier. Conductivity and salinity also increased over the months. The pH, dissolved oxygen concentration and turbidity remained more or less constant throughout the experiment, which was to be expected as the rate of each of these factors was predetermined (it was decided that the reactor would be maintained under anoxic conditions at a more or less neutral pH). The corrosion rate, on the other hand, remained relatively constant throughout the experiment although some peaks were observed. In order to verify these rate values taken by the LPR probe, two other measurement techniques were used, namely a potentiodynamic test and a mass loss measurement on the metal coupons. The latter two methods showed results which, although similar to each other, differed greatly from the results obtained by

the LPR probe. Thus, while the corrosion rate does remain relatively constant over time, it would appear that its value is significantly underestimated by the LPR probe.

As a next step in the experimental process, the values obtained from the placement of the probes in the reactor were analysed in detail in an attempt to understand not only the impact of each of the factors on the corrosion rate of the metal coupons, but also the relationships between these factors. To do this, all the values obtained were plotted and a correlation matrix was produced to facilitate the statistical analysis of the results.

A strong interdependence could be noticed between temperature and conductivity, but also between temperature and salinity. On the other hand, there seemed to be a strong correlation between pH and dissolved oxygen concentration, and also between pH and redox potential. In addition, a strong correlation was observed between salinity and conductivity. Conversely, negative correlations could be observed between certain parameters, in particular between pH and temperature, turbidity and conductivity, but also turbidity and salinity. As far as corrosion rate is concerned, it seems that it increased with an increase in salinity, an increase in conductivity and an increase in temperature. However, a negative correlation could be observed between the corrosion rate and the dissolved oxygen level, but also between this rate and turbidity.

These observations were confirmed by performing a Principal Component Analysis and thus making biplots clearly showing the correlation between each parameter and corrosion.

The final step in the analysis of the results was to place the values obtained on a Pourbaix diagram to graphically represent the pH and potential values at which corrosion occurs.

In addition thereto, a linear polarisation study was carried out in four steps. From this study, a corrosion current as well as a corrosion potential and a polarisation resistance were calculated.

Through these experiments and observations, the influence of various conditions and changes in conditions on the corrosion rate of Grade A steel could be established, and these results can be used in the development of a corrosion prediction system, with the aim of potentially limit corrosion damage. Of course, the results discussed in this thesis are not sufficient for the realisation of such a system and the road is still long.

## Bibliography

- Abdi, H., & Williams, L. J. (2010). Principal component analysis. John Wiley & Sons, Inc. Retrieved from <http://staff.ustc.edu.cn/~zwp/teach/MVA/abdi-awPCA2010.pdf>
- Alahmad, M. (2004). Experimental Study of Scale Formation in Sea Water Environment. *Journal of King Saud University—Engineering Sciences*, 17(1), 73–86. doi:10.1016/S1018-3639(18)30800-6
- Ans, L. (2017, 22 October). Why Stainless steel doesn't Corrode Compared to other Steels. *Steemit*. Accessed 3 April 2021, from <https://steemit.com/science/@lymierikxz/why-stainless-steel-doesn-t-corrode-compared-to-other-steels>
- Ashby, M. F., Shercliff, H., & Cebon, D. (2007). *Materials: Engineering, science, processing and design* (1st ed.). Amsterdam ; Boston: Butterworth-Heinemann.
- ASTM International, & G01 Committee. (n.d.). *Practice for Calculation of Corrosion Rates and Related Information from Electrochemical Measurements*. ASTM International. doi:10.1520/G0102-89R15E01
- Barron, J. J., & Ashton, C. (2007). The Effect of Temperature on Conductivity Measurement, (3), 6.
- Benesty, J., Chen, J., Huang, Y., & Cohen, I. (2009). Pearson Correlation Coefficient. *Noise Reduction in Speech Processing*, Springer Topics in Signal Processing (Vol. 2, pp. 1–4). Berlin, Heidelberg: Springer Berlin Heidelberg. doi:10.1007/978-3-642-00296-0\_5
- Boeckaert, C. (2019, 23 October). KU Leuven works on N removal from greenhouse drainage water in Belgium, Interreg VB North Sea Region Programme. Accessed 31 March 2021, from <https://northsearegion.eu/nuredrain/news/ku-leuven-works-on-n-removal-from-greenhouse-drainage-water-in-belgium/>
- Boundless. (2021, 3 January). Nitrate Reduction and Denitrification. Accessed 1 November 2021, from <https://courses.lumenlearning.com/boundless-microbiology/>
- Caballero, F. G. (2022). *Encyclopedia of materials*. Amsterdam: Elsevier. Retrieved from <http://public.eblib.com/choice/PublicFullRecord.aspx?p=6717697>
- Chang, C., Sommerfeldt, T. G., Carefoot, J. M., & Schaalje, G. B. (2011). Relationships of electrical conductivity with total dissolved salts and cation concentration of sulfate-dominant soil extracts. *Canadian Journal of Soil Science*. NRC Research Press Ottawa, Canada. doi:10.4141/cjss83-008

- Chou, Y. (1975). *Statistical analysis, with business and economic applications* (2d ed.). New York: Holt, Rinehart and Winston.
- Clark, J. (2013, 2 October). Temperature Dependence of the pH of pure Water. *Chemistry LibreTexts*. Accessed 27 October 2021, from [https://chem.libretexts.org/Bookshelves/Physical\\_and\\_Theoretical\\_Chemistry\\_Textbook\\_Maps/Supplemental\\_Modules\\_\(Physical\\_and\\_Theoretical\\_Chemistry\)/Acids\\_and\\_Bases/Acids\\_and\\_Bases\\_in\\_Aqueous\\_Solutions/The\\_pH\\_Scale/Temperature\\_Dependence\\_of\\_the\\_pH\\_of\\_pure\\_Water](https://chem.libretexts.org/Bookshelves/Physical_and_Theoretical_Chemistry_Textbook_Maps/Supplemental_Modules_(Physical_and_Theoretical_Chemistry)/Acids_and_Bases/Acids_and_Bases_in_Aqueous_Solutions/The_pH_Scale/Temperature_Dependence_of_the_pH_of_pure_Water)
- Cole-Parmer. (2021, 21 July). Temperature Effects on Conductivity Measurement. Accessed 21 April 2021, from <https://www.coleparmer.com/tech-article/temperature-effects-on-conductivity-measurement>
- Cunat, P.-J., & Davidson, J. H. (1998). *Working with stainless steels: A manual for craftsmen and technicians*. Paris: SIRPE.
- De Baere, K., Van Haelst, S., Chaves, I., Luyckx, D., Van Den Bergh, K., Verbeken, K., De Meyer, E., et al. (2021). The influence of concretion on the long-term corrosion rate of steel shipwrecks in the Belgian North Sea. *Corrosion Engineering, Science and Technology*, 56(1), 71–80. doi:10.1080/1478422X.2020.1807163
- De Baere, K., Verstraelen, H., Willemen, R., Smet, J.-P., Tchuindjang, J. T., Lecomte-Beckers, J., Lenaerts, S., et al. (2017). Assessment of corrosion resistance, material properties, and weldability of alloyed steel for ballast tanks. *Journal of Marine Science and Technology*, 22(1), 176–199. doi:10.1007/s00773-016-0402-1
- Di Schino, A. (2020). *Manufacturing and application of stainless steels*. S.l.: MDPI AG.
- Dinu, O., & Ilie, A. M. (2015). Maritime vessel obsolescence, life cycle cost and design service life. *IOP Conference Series: Materials Science and Engineering*, 95, 012067. doi:10.1088/1757-899X/95/1/012067
- DNV. (2021 October). DNV-RP-C302: Risk based corrosion management. DNV.
- Duran, B. A. (2013, 8 February). Water hardness effect to galvanized steel corrosion in water. American Galvanizers Association.
- Eberhart, M. E. (2003). *Why things break: Understanding the world by the way it comes apart* (1st ed.). New York: Harmony Books.

- Eijkelkamp Soil & Water. (2017). Multiparameter AP-800—Sensors & Monitoring. Accessed 21 April 2021, from [https://www.eijkelkamp.com/producten/sensors-monitoring\\_nl/multiparameter-ap-800-set.html](https://www.eijkelkamp.com/producten/sensors-monitoring_nl/multiparameter-ap-800-set.html)
- Ferrer, K. S., & Kelly, R. G. (2001). Comparison of Methods for Removal of Corrosion Product from AA2024-T3. *CORROSION*, 57(2), 110–117. doi:10.5006/1.3290336
- Fondriest Environmental, Inc. (2013, 19 November). ‘Dissolved Oxygen’. Fundamentals of Environmental Measurements. *Environmental Measurement Systems*. Accessed 21 April 2021, from <https://www.fondriest.com/environmental-measurements/parameters/water-quality/dissolved-oxygen/>
- Fondriest Environmental, Inc. (2014, 3 March). Conductivity, Salinity & Total Dissolved Solids. Fundamentals of Environmental Measurements. *Environmental Measurement Systems*. Accessed 27 October 2021, from <https://www.fondriest.com/environmental-measurements/parameters/water-quality/conductivity-salinity-tds/>
- González-Viñas, W., & Mancini, H. L. (2004). *An introduction to materials science*. Princeton, N.J: Princeton University Press.
- Groysman, A. (2010). *Corrosion for everybody*. Dordrecht ; New York: Springer.
- Hartmann, K., Krois, J., & Waske, B. (2018). E-Learning Project SOGA: Statistics and Geospatial Data Analysis. Department of Earth Sciences, Freie Universitaet Berlin. Accessed 27 October 2021, from <https://www.geo.fu-berlin.de/en/v/soga/Geodata-analysis/Principal-Component-Analysis/principal-components-basics/Interpretation-and-visualization/index.html>
- Herzberg, E. F., Ambrogio, E. D., Barker, C. L., Harleston, E. F., Haver, W. M., Marafioti, R. J., Stimatze, G. L., et al. (2006). *The annual cost of corrosion for Army ground vehicles and Navy ships* (p. 206). LMI Government Consulting. Retrieved from [http://www.envelopcovers.com/cost-of-corrosion-report-skt50t1\\_final\\_05-01-06.pdf](http://www.envelopcovers.com/cost-of-corrosion-report-skt50t1_final_05-01-06.pdf)
- Heusler, K. E., Landolt, D., & Trasatti, S. (1989). Electrochemical Corrosion Nomenclature. *Pure and Applied Chemistry*, 61(1), 19–22.
- Hou, B., Li, X., Ma, X., Du, C., Zhang, D., Zheng, M., Xu, W., et al. (2017). The cost of corrosion in China. *Npj Materials Degradation*, 1(1), 4. doi:10.1038/s41529-017-0005-2
- Husson, F., Lê, S., & Pagès, J. (2017). *Exploratory multivariate analysis by example using R* (Second edition.). Boca Raton: CRC Press.

- Kaiser, H. F. (1961). A note on Guttman's lower bound for the number of common factors. *British Journal of Statistical Psychology*, 14(1), 1–2. doi:10.1111/j.2044-8317.1961.tb00061.x
- Karabulut, B. (2021). *Fatigue behaviour of duplex welded details*. (Katholieke Universiteit Leuven, Sint-Katelijne-Waver). Retrieved from KU Leuven.
- Kefarge, B., Werkneh, A., Tegegne, A., & Gashaw, F. (2014). An Experimental Study on the Mechanical Characteristics of Low Alloy Carbon Steels for Better Performance of Traditional Farm Implements in Ethiopia. *International Journal of Materials Science and Application*, 3, 420–430. doi:10.11648/j.ijmsa.20140306.31
- Koch, G. H., Brongers, M. P. H., Thompson, N. G., Virmani, Y. P., & Payer, J. H. (2002). *Corrosion Cost and Preventive Strategies in the United States* (p. 786). NACE International.
- Koch, G. H., Varney, J., Thompson, N., Moghissi, O., Gould, M., & Payer, J. (2016). *Interational Measures of Prevention, Application, and Economics of Corrosion Technologies Study* (p. 216). Houston Texas, NACE International. Retrieved from <http://impact.nace.org/documents/Nace-International-Report.pdf>
- Lamarsh, J. R., & Baratta, A. J. (2001). *Introduction to nuclear engineering*. Addison-Wesley series in nuclear science and engineering (3rd ed.). Upper Saddle River, N.J: Prentice Hall.
- Landolfo, R., Cascini, L., & Portioli, F. (2010). Modeling of Metal Structure Corrosion Damage: A State of the Art Report. *Sustainability*, 2(7), 2163–2175. doi:10.3390/su2072163
- Mathiesen, T., Black, A., & Gronvold, F. (2016). Monitoring and Inspection Options for Evaluating Corrosion in Offshore Wind Foundations. *Corrosion*, 11.
- Meyers, M. A., & Chawla, K. K. (1999). *Mechanical behavior of materials*. Upper Saddle River, N.J: Prentice Hall.
- Mittemeijer, E. J. (Ed.). (2015). *Thermochemical surface engineering of steels*. Woodhead publishing series in metals and surface engineering. Amsterdam: Woodhead Publishing.
- Nguyen Le, T. (2017, 1 November). Stainless Steel Material In Sea Water. *General Technical knowledge*. Retrieved from

<https://shipbuildingknowledge.wordpress.com/2017/11/01/stainless-steel-material-in-sea-water/>

Nickel Development Institute, & Specialty Steel Institute of North America. (n.d.). Design Guidelines for the Selection and Use of Stainless Steels.

Nordstrom, D. K., & Wilde, F. D. (2005). *Reduction Oxidation Potential (Electrode Method)*.

Ødegaard, H. (2006). Innovations in wastewater treatment: –The moving bed biofilm process. *Water Science and Technology*, 53(9), 17–33. doi:10.2166/wst.2006.284

Outokumpu. (2020). Supra 316L/4404 EN 1.4404, ASTM TYPE 316L / UNS S31603 stainless steel grade details. Accessed 3 April 2021, from <https://secure.outokumpu.com/steelfinder/Properties/GradeDetail.aspx?OKGrade=4404&Category=Supra>

PalmSens. (2021a). Tafel Plot and Evans Diagram. *PalmSens*. Accessed 27 October 2021, a from <https://www.palmsens.com/knowledgebase-article/tafel-plot-and-evans-diagram/>

PalmSens. (2021b). Evans Diagram. *PalmSens*. Accessed 27 October 2021, b from <https://www.palmsens.com/knowledgebase-topic/evans-diagram/>

Pawlowicz, R. (2013). Key Physical Variables in the Ocean: Temperature, Salinity, and Density | Learn Science at Scitable. Accessed 23 October 2021, from <https://www.nature.com/scitable/knowledge/library/key-physical-variables-in-the-ocean-temperature-102805293/>

Pedefferri, P. (2018). *Corrosion Science and Engineering*. Engineering Materials (1st ed. 2018.). Cham: Springer International Publishing : Imprint: Springer. doi:10.1007/978-3-319-97625-9

Peres-Neto, P. R., Jackson, D. A., & Somers, K. M. (2005). How many principal components? Stopping rules for determining the number of non-trivial axes revisited. *Computational Statistics & Data Analysis*, 49(4), 974–997. doi:10.1016/j.csda.2004.06.015

Pourbaix, M. J. N., De Zoubov, N., & Van Muylder, J. (1963). *Atlas d'équilibres électrochimiques*. Publication du Centre belge d'étude de la corrosion. Paris: Gauthier-Villars.

- Reagecon. (n.d.). Reagecon Producer of Physical & Chemical Standards. Accessed 27 October 2021, from <https://www.reagecon.com/en-gb/>
- Reid, R. N. (2020). *Water quality systems: Guide for facility managers*. Retrieved from <https://www.taylorfrancis.com/books/9781003151081>
- Roberge, P. R. (2008). *Corrosion engineering: Principles and practice*. New York: McGraw-Hill.
- Sarja, A. (2000). Durability design of concrete structures—Committee report 130-CSL. *Materials and Structures*, 33(1), 14–20. doi:10.1007/BF02481691
- Savitzky, A. (1989). A Historic Collaboration. *Analytical Chemistry*, 61(15), 921A-923A. doi:10.1021/ac00190a744
- Speight, J. G. (2014). *Oil and gas corrosion prevention: From surface facilities to refineries* (Online-Ausg.). Waltham, Massachusetts Oxford, England: Gulf Publishing Company.
- Steel Construction Institute (Great Britain). (2017). *Design manual for structural stainless steel* (4th ed.). Ascot, UK: Steel Construction Institute.
- Thompson, M. L., & Kateley, L. J. (1999). The Nernst Equation: Determination of Equilibrium Constants for Complex Ions of Silver. *Journal of Chemical Education*, 76(1), 95. American Chemical Society. doi:10.1021/ed076p95
- Van Aken, P. (2021). *Nitrate removal from drainage water and greenhouse effluent*. Presented at the Interreg North Sea Region - NuReDrain, Belgium.
- Van Praet, S. (2020 2021). *Toepassing van de MBBR-technologie om nitraat te reduceren uit drainagewater*. (Katholieke Universiteit Leuven, Sint-Katelijne-Waver).
- Vernier Software and Technology. (n.d.). Chloride and Salinity. *Vernier*. Accessed 21 April 2021, from [https://www.vernier.com/experiment/wqv-15\\_chloride-and-salinity/](https://www.vernier.com/experiment/wqv-15_chloride-and-salinity/)
- Young, F. W. (1999). Principal Components: BiPlots. Retrieved from <https://www.uv.es/prodat/ViSta/vista-frames/help/lecturenotes/lecture13/biplot.html>
- YSI Incorporated. (2021). ORP - Oxidation Reduction Potential or Redox Measurement in Water Explained. Accessed 23 October 2021, from <https://www.yei.com/parameters/orp-redox>